Characterization of $Y_3(Al,Ga)_5O_{12}:Ce^{3+}$ phosphor thin films prepared by Pulsed Laser Deposition

by

Sipho Thapo Solomon Dlamini

(B.Sc Hons)

A thesis submitted in fulfillment of the requirements for the degree

MAGISTER SCIENTIAE

In the

Faculty of Natural and Agricultural Sciences

Department of Physics

at the

University of the Free State

Republic of South Africa

Promoter: Prof H.C. Swart

Co-promoter: Prof O.M. Ntwaeaborwa

November 2013

This thesis is dedicated to my parents, my late father, Tjabulane David Dlamini and my mother Mamqebozo Letia Dlamini.

Acknowledgements

- To the One in charge of my life, Jesus Christ, thank you for all things.
- My promoter Prof H.C. Swart for his professional leadership and overwhelming support during the duration of my studies.
- My co-promoter Prof O.M. Ntwaeaborwa for advices he gave regarding my research and about life in general.
.
- Brian Yalisi at the National Laser Center for his assistance with preparation of films using the PLD.
- Philip of the iThemba labs for RBS measurements.
- Hanlie Grobler and Prof van Wyk of the Center for Microscopy UFS for their assistance with SEM images.
- Personnel at the Physics Department for discussions and assistance.
- To my mom and my late father who both gave me their unconditional love, I owe this to them. Thank you for all the sacrifices.
- To my brothers, Jabu and Themba for pushing me to do my best.
- To my lovely little sisters, Thandeka and Khethiwe for putting a smile on my face.
- And to Letlotlo, for bringing more love and meaning to my life. You are special.

Abstract

The morphological and luminescent properties of $Y_3(Al,Ga)_5O_{12}:Ce^{3+}$ powder phosphor were investigated. Scanning Electron Microscopy (SEM) revealed the phosphor's agglomerated particles with a size ranging from 0.4µm to 1.4µm. The X-ray diffraction (XRD) indicated a cubic polycrystalline phosphor with an average crystal size of 80 nm. Excitation peaks for the powder were obtained at 439, 349, 225 and 189 nm and emission peaks at 512 and 565 nm. Emission wavelength at 512 nm was also used to approximate the Al/Ga ratio within the crystal. Photoluminescence (PL) data also revealed that the addition of the Ga into the $YAG:Ce^{3+}$ matrix caused a blue-shift in the emission spectra. The UV-VUV excitation and emission spectra of the $Y_3(Al,Ga)_5O_{12}:Ce^{3+}$ were also recorded and an energy diagram was constructed from the values.

The phosphor powder was used as target material for Pulsed Laser Deposition (PLD). SiO_2/Si(100) was used as substrates and thin films were deposited in the presence of different background gases. XRD indicated that better crystallization took place for films deposited in a 20 mTorr O_2 atmosphere. Atomic force microscopy (AFM) revealed an RMS value of 0.7 nm, 2.5 nm and 4.8 nm for the films deposited in vacuum, O_2 and Ar atmospheres, respectively. The highest PL intensity was observed for films deposited in the O_2 atmosphere. The thickness of the films varied from 120 nm to 270 nm with films deposited in vacuum having the thin layer and those in Ar having the thick layer. The stoichiometry of the powder was maintained in the film during the deposition as confirmed by Rutherford backscattering spectroscopy (RBS).

Luminescent properties of $Y_3(Al,Ga)_5O_{12}:Ce^{3+}$ thin films prepared by PLD at different substrate temperatures in an O_2 background atmosphere were also investigated. XRD indicated that the films have the same cubic polycrystalline phase structure as the powder. AFM revealed poorly defined grain growth for films ablated at a substrate temperature of 22°C and 500°C but well

defined grain growth was observed for films ablated at a 300°C substrate temperature. Auger electron spectroscopy (AES) depth profile of the film ablated at 500°C indicated that Si has diffused into the thin film. The highest PL intensity was observed for films deposited at the substrate temperature of 300°C. A slight shift in the wavelength of the PL spectra was obtained for the thin films with respect to the powder due to a change in the crystal field.

The maximum PL intensity was obtained from the film deposited at the substrate temperature of 300^{0}C in an O_2 atmosphere. In addition, the films with well-defined grains (rougher surfaces) showed higher PL intensity compared to films with poorly-defined grains (smooth surfaces) as confirmed from AFM data

Keywords: $Y_3(Al,Ga)_5O_{12}:Ce^{3+}$; Pulsed Laser Deposition; different gas atmospheres, substrate temperature, photoluminescence.

Table of Contents

Chapter 1

Introduction

For the past few years, there has been much attention given to phosphors based on Eu^{2+} or Ce^{3+} activator ions for solid state lighting application [1-6]. These ions are characterized by d-f transitions which are extremely intense. Ce^{3+}-doped compounds generally show an emission in the near UV [7], but in the presence of high crystal fields such as in garnets, visible emissions are observed [8]. Ce-doped $Y_3Al_5O_{12}$ (YAG:Ce) is such a garnet. YAG:Ce^{3+} shows yellow emission from the characteristic 5d-4f transitions of Ce^{3+} ion, and these energy levels of the Ce^{3+} ion strongly depend on the host's crystal field which induces the energy level splitting of $5d^1$ orbital. YAG:Ce has numerous applications such as a luminescent material in plasma display panels (PDPs) [9], solid state lighting, scintillators and thermographic phosphor [10][11][12]. Recently the Ce^{3+}-doped garnet phosphors have attracted a great deal of attention in the application for white light emitting diodes (LEDs). The first generation of white lamps is based on a combination of the InGaN chip emitting blue photons at around 480 nm, coated with a broad-band yellow Ce^{3+} doped yttrium aluminum garnet (YAG: Ce) phosphors [13]. Usually the InGaN chip is covered by a layer of YAG:Ce phosphor which converts some of the blue light into yellow light. This blue LED plus yellow phosphor combination gives a cool white light. This white LEDs are already widely used as back-lighting in cellphones as interior lighting in aircraft, cars and buses and as bulbs in flash lights. However the quality of this white light is not good enough for home and office lighting for which a warmer white light is desirable which means adding some red light to the blue plus yellow combination. Unfortunately very few red phosphor material are available for excitation using blue or near UV light and those that are available have a low efficiency. Phosphors for LED lighting are being produced. One of these

phosphors is Cerium-doped yttrium aluminum gallium garnet (YAGG: Ce). It is a modified form of the more traditional YAG:Ce. In YAG:Ce, Al^{3+} is often replaced with Ga^{3+} because of the similarity in cation size and because the addition of Ga^{3+} induces changes in the photoluminescence (PL) spectra. Wu et al [14] showed that increasing the amount of Ga^{3+} in YAG:Ce blue-shifts the emission due to lattice distortions around the rare-earth ion and this results are useful to the development of red phosphors for solid state lighting devices such as the LEDs. YAGG:Ce phosphors is normally obtained in ultrafine powder form by being synthesized by wet chemical methods such as co-precipitation, sol-gel, combustion and hydrothermal methods. The yellow phosphor blue LED combination to produce white light has short comings as mentioned earlier, it is difficult to obtain a uniform emission of white light from this combination. To overcome the weakness of using mixtures of phosphor powders and LEDs, thin film phosphor has been used to convert primary light from LEDs in LED-phosphor lighting. In LED-phosphor lighting applications, phosphors in a thin film form support better methods of fabrication of white lighting system and can be more conveniently integrated with LEDs and arrays of LEDs than those of the powder type [15,16].

In preparation of thin films, Pulsed Laser Deposition (PLD) is one of the best preparation techniques. The advantages of the PLD technique include the following: PLD is a “pulsed” process by which the number of particles arriving at the substrate can be controlled precisely with the number of pulses and the fluence. Therefore layer-by-layer growth can be achieved by adjusting the number of arriving atoms to the number of atoms in a monolayer, and thus that highly perfect surfaces and interfaces in sandwich-systems can be produced from a bulk target of similar stoichiometry. The laser-target interaction which initiates the ablation process is completely decoupled from other process parameters such as background pressure, type of

background gas and substrate temperature. Other process parameters which have a significant influence on the properties of laser ablated thin films include laser fluency, laser wavelength, laser energy, shape of the laser pulse, number of pulses, repetition rate, laser type, etc.

1.1. Problem statement

$Y_3(Al_2,Ga_3)O_{12}:Ce^{3+}$ (YAGG:Ce) has been extensively investigated in powder form. There is however very limited reports in the literature on YAGG:Ce thin films. There is only few reports in literature on the elemental composition and structural analysis of PLD YAGG:Ce thin films. The investigation on the influence of different PLD deposition parameters on the properties of YAGG:Ce thin films is crucial because YAGG:Ce films have a potential to be applied in the production of white LEDs that are bright enough to be used for home and office lighting.

1.2. Research objectives:

- To characterize the morphological and luminescent properties of YAGG:Ce^{3+} powder phosphor.
- To prepare YAGG:Ce^{3+} thin films using the PLD technique.
- To study the changes in morphological and luminescent properties of the thin films with change in PLD deposition parameters.
- To study the structural and morphological properties of thin films prepared by PLD using XRD, AFM, SEM, AES and RBS.
- To study the luminescent properties of YAGG:Ce^{3+} thin film prepared by PLD using PL.

1.3. Thesis Layout

Chapter 2 provides an overview to phosphors and their basic principles as well as introduction to the PLD technique. Chapter 3 is an overview of the characterization techniques. Morphological and luminescent properties of $Y_3(Al,Ga)_5O_{12}:Ce^{3+}$ phosphor in powder form are discussed in Chapter 4. Chapter 5 and 6 addresses the effects of different atmospheric gas atmospheres and substrate temperature on the structure, morphology and PL properties of PLD $Y_3(Al,Ga)_5O_{12}:Ce^{3+}$ nano thin films. PL properties of Y_3 (Al, Ga)$_5O_{12}:Ce^{3+}$ thin phosphor films grown by PLD at various deposition parameters are investigated and summarized in Chapter 7. Chapter 8 gives the summary of the thesis result and suggestions for future work. The last part of the thesis gives a list of publications resulting from this work and the conferences presentations

1.4. References

[1] Y.Q. Li, A.C.A. Delsing, G de With, H.T. Hintzen, Chem. Mater. 17 (2005) 3242

[2] Y.Q. Li, J. Alloys Compd. 417 (2006) 273

[3] J.K. Park, K.J. Choi, K.N. Kim, C.H. Kim, Appl. Phys. Letter. 87 (2005) 031108

[4] S. Neeraj, N. Kijima, A.K. Cheetham, Solid State Commun. 131 (2004) 65

[5] S. Neeraj, N. Kijima, A.K. Cheetham, Chem. Phys. Lett. 287 (2004) 2

[6] R. Le Toquin, A.K. Cheetham, Chem. Phys.Lett. 423 (2006) 352

[7] G. Blasse, B.C. Grabmeier, Luminescent Materials, Springer, Berlin, 1994.

[8] G. Blasse, A. Bril, Appl. Phys. Lett. 11 (1967) 53

[9] T. Kojima, S. Shionoya, W.M. Yen (Eds), Phosphor Handbook, CRC Press, New York, 1998, p. 628

[10] G. Xia, S. Zhou, J. Zhang, J. Xu, Jounal of Crystal Growth. 279 (2005) 357–362

[11] S.W. Allisson, G.T. Gillies, Rev. Sci. Instrum. 68(7) (1997) 2615

[12] J. Tous, K. Blazek, L. Pina, B. Sopko, Radia. Meas. 42 (2007) 925

[13] P. Schlotter, R. Schmidt, J. Schneider, Appl. Phys. A. 64 (1997) 417

[14] J.L Wu, G. Gundiah, A. Cheetham, Chem. Phys. Lett. 441 (2007) 250

[15] J.Y. Choe, Mater. Res. Innov. 6 (2002) 238-241

[16] R.B. Mueller-Mach, G.O. Mueller, U.S. Patent 7183577 B2 (2007)

Chapter 2

Theory

2.1. Introduction to Phosphors

A phosphor is a material capable of absorbing energy and re-emitting it in the form of light (Ultra-Violet, Visible or Infra-Red) in a phenomenon known as luminescence. Most phosphors are usually made up of a host material (matrix) and dopant. The host material is normally an insulator or a semiconductor with a wide band gap and it serves to accommodate the dopant. The host also controls some of the physical properties of the phosphor. A dopant (usually a rare earth) is added as an activator for luminescence. An activator is an impurity ion which is added intentionally into the host material to give rise to a center that can be excited to luminescence. Dopants have a different electron orbital structure compared to the host material. Therefore, in regions of the host around the dopant ion, additional energy levels that can accommodate electrons or holes become available. These levels can be close to the conduction band, in which case the dopant is called a donor, or close to the valence band, in such case it is called an acceptor. Transitions between these levels can give rise to luminescence in such case the dopant is known as an activator. In most cases, the activator is present in extremely small concentrations, ranging from as much as one dopant atom in 5000 host atoms down to as little as one dopant atom in 1 million host atoms. Luminescence is defined as the radiation emitted by a molecule, or an atom, after it had absorbed energy to go to an excited state. If the absorbed energy or source of excitation is in the form of a photon then the process is known as photoluminescence.

2.2. Photoluminescence

Absorption of an ultraviolet or visible photon promotes a valence electron from its ground state to an excited state with conservation of the electron' spin. For example, a pair of electrons occupying the same electronic ground state have opposite spins (Figure 2.1(a)) and are said to be in a singlet spin state. Absorbing a photon promotes one of the electrons to a singlet excited state (figure 2.1(b)).

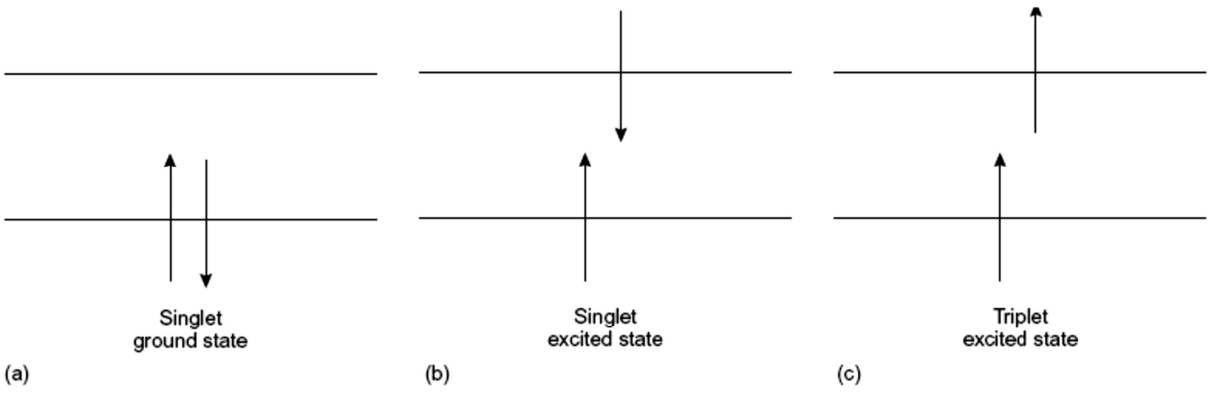

Figure 2.1: The ground and excited state of a molecule [1]

This phenomenon is called "excitation". In a triplet state however, the excited electron is no longer paired with the ground state electron, they now have the same spin. Since excitation to a triplet state involves an additional spin transition, it is more probable that an excited singlet will form upon absorption of a photon. The excited states are not stable and will not stay indefinitely. At some random moment, a molecule in the excited state will spontaneously return to the ground state. This return process is called decay, deactivation or relaxation. The energy absorbed during the excitation process can be released during the relaxation in the form of a photon. This type of relaxation is called emission and it can be divided into two emission types: Flourescence and Phosphorescence (see section 2.2.1.2 and2.2.1.3).

A molecule in the excited state can decay or relaxes in several ways. If the molecule initially occupies the lowest vibrational energy level of its electronic ground state. The ground state, which is shown in figure 2.2, is a singlet state labeled S_0. Absorption of a photon of correct energy excites the molecule to one of several vibrational energy levels in the first excited electronic state, S_1, or the second electronic excited state, S_2, both of which are singlet states. Relaxation to the ground state from these excited states occurs by a number of mechanisms that are either radiationless, in that no photons are emitted, or involve the emission of a photon. These relaxation mechanisms are shown in figure 2.2.

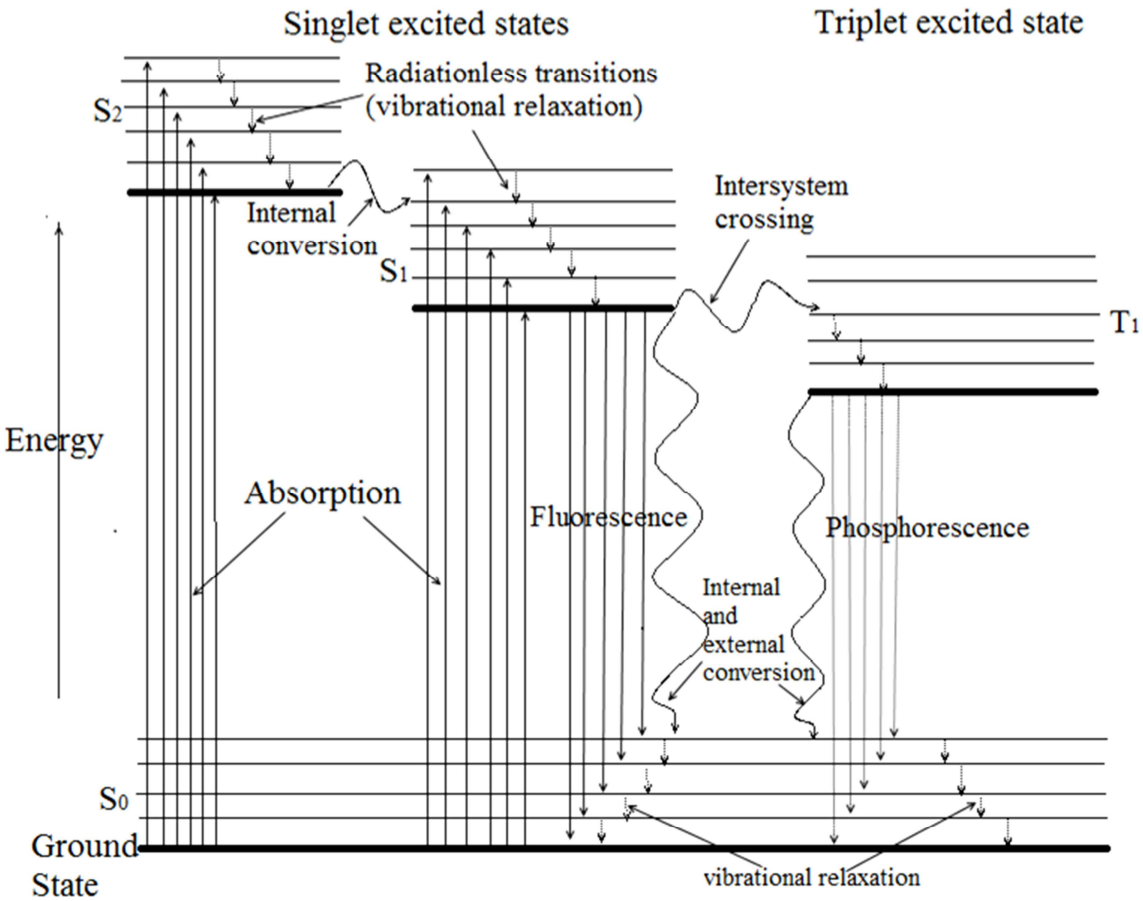

Figure 2.2: Partial energy diagram for a photoluminescence system (Jablonski diagram) [2]

2.2.1. Mechanism taking place in Photoluminescence

2.2.1.1 Radiationless transitions

One form of radiationless transitions is vibrational relaxation**,** in which a molecule in an excited vibrational energy level loses energy as it moves to a lower vibrational energy level in the same electronic state. Vibrational relaxation is very rapid, with the molecule's average lifetime in an excited vibrational energy level being 10^{-14} to 10^{-13} [3]. Because if this, molecules that are excited to different vibrational energy levels of the same excited electronic state quickly return to the lowest vibrational energy level of the same excited state. Another form of radiationless relaxation is internal conversion**,** in which a molecule in the ground vibrational level of an excited electronic state passes directly into a high vibrational energy level of a lower energy electronic state of the same spin state [4]. For example transitions from S_2 to S_1 (See figure 2.2). Therefore a molecule in an excited electronic state may return or relaxes to the ground electronic state without emitting a photon by undergoing internal conversions and vibrational relaxations.

A final form of radiationless relaxation is an intersystem crossing in which a molecule in the ground vibrational energy level of an excited electronic state passes into a high vibrational energy level of a lower energy electronic energy state with a different spin state. For example, transitions from S_1 to T_1 as shown in figure 2.2 [4].

2.2.1.2 Fluorescence

Fluorescence occurs when a molecule in the lowest vibrational energy level of an excited electronic state returns to a lower energy electronic state by emitting a photon. Since molecules return to their ground state by the fastest mechanism, fluorescence is only observed if it is a more efficient means of relaxation than the combination of internal conversion and vibrational

relaxation. Fluorescence emission of photons stops immediately when excitation is cut off. Also in fluorescence there are no traps but many luminescent centers. To summarize, the process of fluorescence consist of photon absorption by a molecule to go to an excited singlet state, relaxation from higher vibrational levels of that state to its lowest vibrational level, photon emission to a vibrationally exited level of the ground state, and again relaxation of the molecule to the lowest vibrational level of the ground state. The lifetime of an excited singlet state is approximately 10^{-9} to 10^{-8} sec and therefore the decay time of fluorescence is of the same order of magnitude [3].

2.2.1.3. Phosphorescence

Although population of triplet states by direct absorption from the ground state is highly unlikely, a more efficient process exists for population of triplet states from the lowest excited singlet state in many molecules. This process is referred to as intersystem crossing, and is a spin-dependent internal conversion process. The mechanism for intersystem crossing involve vibrational transitions between the excited singlet state and a triplet state. This are transitions from S_1 to T_1 as shown in figure 2.2. Once intersystem crossing has occurred the molecule undergoes the usual internal conversion process as described in section 2.2.1.1 and falls to the lowest vibrational level of the triplet state. A radiative transition between the lowest triplet state and the ground state then takes place. This emission is called phosphorescence [4]. As phosphorescence originates from the lowest triplet state, it will have a decay time approximately equal to the lifetime of the triplet state (10^{-4} to 10 sec or more). Therefore phosphorescence is often characterized by an afterglow which is not observed in fluorescence.

2.2.2 Excitation and Emission Spectra

Photoluminescence spectra are recorded by measuring the intensity of emitted radiation as a function of either the excitation wavelength or the emission wavelength. In an excitation spectrum the emission light is held at a constant wavelength, and the excitation light is scanned through many different wavelengths (via a monochromator). In an emission spectrum a fixed wavelength is used to excite the molecules, and the intensity of emitted radiation is monitored as a function of wavelength.

2.3 Other types of Luminescence

Cathodoluminescence:

Is a phenomenon where electrons impacting on a luminescent material such as a phosphor, cause the emission of photons which may have wavelengths in the visible spectrum. A familiar example is the generation of light by an electron beam scanning the phosphor-coated inner surface of the screen of a television that uses a cathode ray tube. Cathodoluminescence is the inverse of the photoelectric effect in which electron emission is induced by irradiation with photons.

Electroluminescence:

Is an optical phenomenon and electrical phenomenon in which a material emits light in response to the passage of an electric current or to a strong electric field.

Thermoluminescence:

Is a form of luminescence that is exhibited by certain crystalline materials, such as some minerals, when previously absorbed energy from electromagnetic radiation or other ionizing radiation is re-emitted as light upon heating of the material.

Bioluminescence:

Is the production and emission of light by a living organism. Bioluminescence occurs widely in marine vertebrates and invertebrates, as well as in some fungi, microorganisms and terrestrial invertebrates.

Electrochemiluminescence:

Is a kind of luminescence produced during electrochemical reactions in solutions.

Mechanoluminescence:

Is light emission resulting from any mechanical action on a solid. It can be produced through ultrasound, or through other means.

Radioluminescence:

Is the phenomenon by which light is produced in a material by bombardment with ionizing radiation such as beta particles.

2.4. Phosphors for LEDs

Most phosphors have been developed for use with fluorescent tubes or Compact florescence lamps (CFLs) that emit UV radiation, and hence, they have not been optimized for use with LEDs emitting in the visible spectrum [5]. The first commercially available white LED was based on an InGaN chip emitting blue light at a wavelength of 460 nm that was coated with a $Y_3Al_5O_{12}:Ce^{3+}$ (YAG:Ce) phosphor layer that converted some of the blue light into yellow light [6]. Both the chip and the phosphor are nontoxic, so the white LED is not toxic (unlike CFLs). The blue LED plus yellow phosphor combination just outlined gives a cool white light.

2.4.1. Solid-State Lighting and LEDs

This next generation of home and office lighting will almost certainly be inorganic LEDs. LEDs are semiconductors in which the light emission comes from a very thin crystalline layer composed of typically two, three, or four elements such as indium gallium nitride (InGaN). This very thin layer, typically only about five atomic layers, or 2 nm, thick, is called a quantum well. The quantum well of InGaN is sandwiched between two thicker layers of gallium nitride (GaN), one of which, called *n*-type GaN, is rich in negatively charged particles called electrons, and the other, called *p*-type GaN, is rich in positively charged particles called holes. When a voltage, for example, from a battery, is applied across the sandwich, electrons are injected into the InGaN quantum well from the *n*-type GaN, and holes are injected from the *p*-type GaN. These electrons and holes exist in the InGaN at different energy levels separated by an energy bandgap. When the electrons and holes subsequently meet and recombine, the energy released is given out as light, and the wavelength of the light emitted is equivalent to the bandgap energy. This results in the emission of light of a single color, such as red or green or blue, called monochromatic light. This color can be changed by varying the composition of the InGaN quantum well and also by changing the thickness of the quantum well. Scientists are therefore able to make an LED emit light of any desired color. This tailor-made lighting has become possible only recently because of some fundamental advances in materials science, and it is revolutionizing the field of lighting [5].

2.4.2 Phosphors for LED-based Lighting

Recently attention has been paid on YAG:Ce because it can be applied to white LEDs as yellow emission phosphors. The Ce^{3+} ion is responsible for nanosecond decay times and an intense yellow-green emission wavelength [7]. Trivalent Ga atoms have been substituted for Al atoms in

order to blue-shift the emission wavelength for use in solid-state light applications such as fabrication of white LEDs. The most common method to produce white light with LEDs is the combination of blue InGaN-GaN LEDs with the yellow emitting YAG:Ce phosphor. With a LED emission wavelength of 440 – 470 nm a fraction of the LED emission is absorbed by the YAG:Ce phosphor and down-converted to the well-known broad yellow emission of the phosphor. YAG:Ce absorbs blue LED radiation through the allowed $4f^1 \rightarrow 5d^1$ transition and emits yellow light via the reverse $5d^1 \rightarrow 4f^1$ transition. The emission from the lowest excited $5d^1$ level is to the spin–orbit split $4f^1$ ground states, leading to an extremely broad emission band. Not converted blue LED light and the yellow emission are mixed by the phosphor powder layer to obtain white light in a wide range of correlated color temperatures (CCT) from 4000 – 8000 K [8]. This enables LEDs to be used in many applications where color quality is not a key requirement, including backlights for portable displays, indicators, bicycle lights, in large display screens, as the interior lighting in cars, buses, trains, and planes; or as the exterior lighting on buildings. Besides being applied in solid state lighting application, YAG:Ce can also be applied in scintillators and as a thermographic phosphors (TGP) for use in non-contact thermometers [9-12].

2.5. $Y_3(Al,Ga)_5O_{12}:Ce^{3+}$ (YAGG:Ce) phosphor

Cerium-doped yttrium aluminum gallium garnet ($Y_3(Al,Ga)_5O_{12}:Ce^{3+}$/YAGG:Ce) powder phosphor is a modified form of the more traditional yttrium aluminum garnet ($Y_3Al_5O_{12}:Ce^{3+}$/YAG:Ce) phosphor. In YAG, 3.75 atoms of Ga are substituted with 1.25 atoms of Al on average for YAGG:Ce. YAG:Ce is used in several applications such as solid-state lighting, displays, scintillators, and thermographic phosphors (TGP)[13]. YAG is transparent and colorless in the visible range. YAG's optical bandgap is in the order of 6.6 eV, with the

valence band comprised of filled oxygen 2p orbitals, and the conduction band comprised of empty yttrium 4d orbitals. The UV absorption between 300 nm and the band edge at 190 nm varies dramatically from crystal to crystal [14]. YAG:Ce^{3+} mainly belongs to the luminescent materials with individual luminescent centers. The Ce^{3+} ion has only one electron in the 4f state. The ground state is split into a $^2F_{5/2}$ and a $^2F_{7/2}$ level by the spin-orbit interactions. The first excited state originates from the 5d state, which interacts strongly with the host lattice due to the large spatial extent of the 5d wave function. Thus the crystal-field interaction dominates over the spin-orbit interaction and the 4f to 5d transitions are parity and spin allowed [15]. When a Ce^{3+} ion enters exclusively one specific lattice site, its 5d state will be split into 2–5 different components depending on the site symmetry [16]. The 5 d state may also split into several more components if present in more than one lattice position with different site symmetry. Ce^{3+} doped phosphors typically have two emission bands due to the true levels of $^2F_{5/2}$ and $^2F_{7/2}$ of the 4f configuration of Ce^{3+} [17,18]. Coetsee et. al. [19] found that the cathodoluminescent (CL) and PL emission spectra for Y_2SiO_5:Ce^{3+} phosphor powder due to the Ce^{3+} ions were attributed to the two different sites (A1 and A2) of the Ce^{3+} ion in the host matrix and the difference in the orientation of the neighbor ions in the complex crystal structure. Each Ce^{3+} site gave rise to transitions from the 5d to the two (therefore two peaks) 4f energy levels ($^2F_{5/2}$ and $^2F_{7/2}$ due to crystal field splitting). For the understanding of the lanthanide fd structure, knowledge about the excitation spectrum of the Ce^{3+} ion in a certain host lattice is very important. The Ce^{3+} ion has the $4f^1$ configuration, and irradiation with UV radiation will excite this 4f electron into a 5d orbital, leaving the 4f shell empty. Therefore, the excitation spectrum of Ce^{3+} will give direct information on the crystal-field splitting of the 5d orbitals. A similar crystal-field splitting is expected for all rare-earth ions in the same host lattice. The crystal-field splitting of the 5d states

dominates the structure in the fd excitation spectra, even in the more complex rare-earth ions with more than one 4f electron cases [20].

As stated earlier, YAGG:Ce is a modified form of the more traditional YAG:Ce where Ga ions are substituted for some Al ions. YAG has a strong emission wavelength at around 540 nm [21] but YAGG:Ce has a strong emission at around 512 nm [22] and this is due to the presence of gallium in the YAG matrix which shifts the peak positions to lower diffractions angles because of the difference in radius size of Al and Ga ions. Ga ion is larger than Al ion by about 20.5 % in the tetrahedral sites and 17 % in the octahedral sites [23]. The addition of Ga ion into the YAG structure is influential on the environment of the Ce^{3+}. Ultimately, the substitution of Ga into the YAG lattice result in a decompression of oxygen atoms directly coordinated to the Ce^{3+} atom and the structure becomes more cubic. This change in structure directly affect the 5d orbitals of the Ce^{3+} and likewise the photoluminescent characteristics.

2.5.1 The crystal structure of $Y_3(Al,Ga)_5O_{12}:Ce^{3+}$ (YAGG:Ce) phosphor

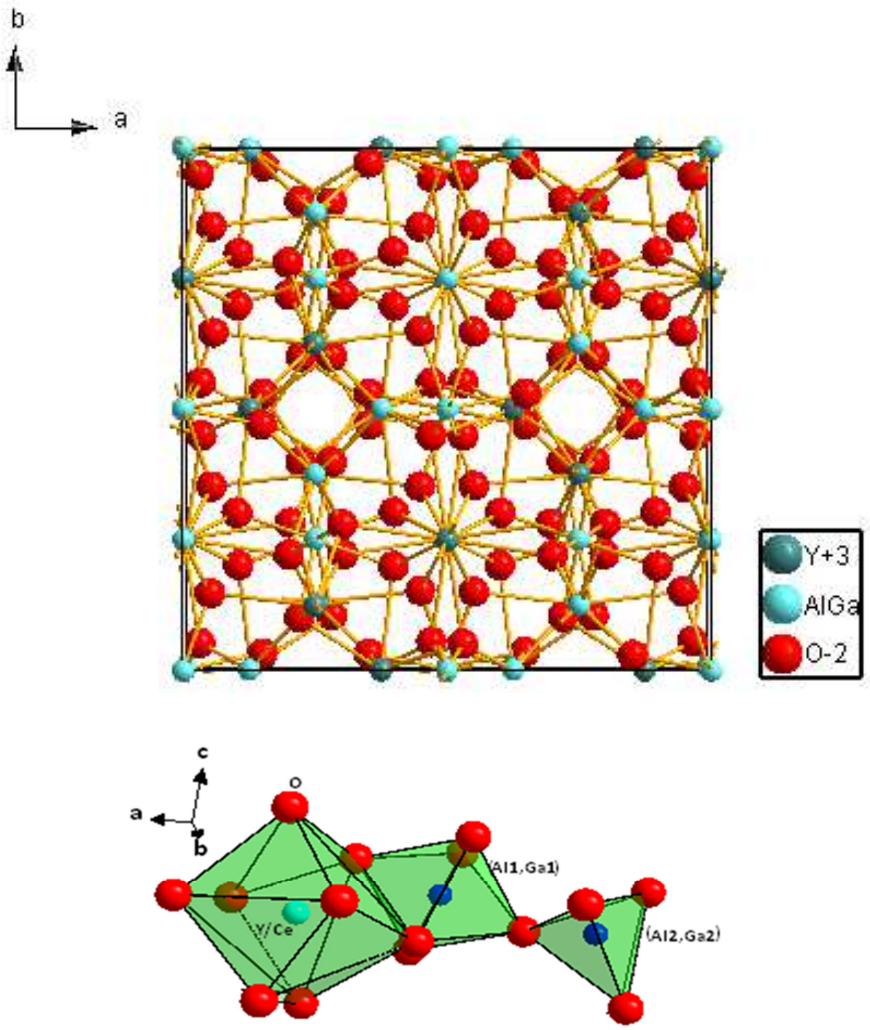

Figure 2.3: The relative arrangement of Y, O, Al and Ga in $Y_3(Al,Ga)_5O_{12}:Ce^{3+}$ [24]

The schematics of the relative arrangement of Y, O, Al and Ga were drawn using the diamond crystal software [24] and are shown in figure 2.3. The Y/Ce ions are surrounded by O^{2-} ions in the dodecahedral arrangement. The Al^{3+} and Ga^{3+} are surrounded by O^{2-} ions in a tetrahedral and octahedral arrangement.

2.6. PLD and thin film growth

It has been shown that YAGG:Ce has characteristics that are suitable for this phosphor to be applied for the fabrication of LEDs [25]. However in literature YAGG:Ce has been studied rather extensively in the powder form but not so much in the thin film form. Particularly thin films that have been prepared by the pulsed laser deposition (PLD) technique did not gain much attention in the past. Thin films offers several advantages due to their good luminescence characteristics, higher image resolution from small grains, better thermal stability and good adhesion to the substrate [26].

PLD is a well-known fast and effective technique to grow phosphor thin films. However the intensity is still the problem due to particle formation. One of the solutions to the particle formation problem is optimization of the laser process parameters such as the background gas pressure (oxygen), laser fluence, laser pulse frequency, number of pulses, substrate temperature and the target to substrate distance. Surface morphology and thickness can be controlled by varying the growth parameters [27, 28]. The luminescent intensity of phosphor thin films can strongly depend on the surface morphology. A rougher surface would increase the intensity due to a lesser effect of total internal reflection if compared to a smooth thin film surface [29].

2.7. Advantages of the PLD:

Compared to other thin film growth techniques, the PLD has the following advantages.

- It is a versatile technique. A wide range of materials such as oxides, metal, semiconductors and even polymers can be grown by PLD.
- It has the ability to maintain target composition in the deposited thin films, keeping the stoichiometry of the target.
- Deposition can occur in both inert and reactive background gasses.

2.8. Disadvantages of the PLD:

- The generation of particulates during the deposition process, which are not ideal for the application field.
- The non-uniform layer thickness.
- The ablation plume cross section is generally small and this limits the sample size.

2.9. Influence of PLD parameters on the growth of oxide thin films

Pulsed laser deposition (PLD) is one of the most widely used growth techniques for oxide thin films. In 1987, Dijkkamp et al. showed that the composition of the PLD-grown $YBa_2Cu_3O_7$ oxide films was close to that of the bulk target.[30]. Recently complex oxide such as $Ba_2Co_2Fe_{12}O_{22}$ have been grown using PLD [31]. The stoichiometric removal of material from a solid target is the single most important factor in the success of PLD. PLD parameters such as fluency, background gas and substrate temperature are key for stoichiometric removal and transfer and can be used to control the stoichiometry. The laser–solid interaction mechanisms may depend on the laser wavelength. The most important effect of the laser's wavelength is its determination of the penetration depth. Most of the energy should be absorbed in a very shallow layer near the surface of the target to avoid subsurface boiling, which can lead to a large number of particulates at the film surface. Lasers with long pulse duration have a strong interaction with the plume. This result in films ablated with long pulsed duration (KrF 248 nm, ≈25 ns pulse duration) being superior compared to those ablated with a relatively shorter pulsed duration interaction (Nd:YAG 266 nm, ≈ 5 ns pulse duration) with the plume [32].

2.9.1. Fluence

In PLD, fluence is the parameter that controls the energy of the laser as well as the spot of the laser on the target sample. Particles' number density depends on the fluency. The particle number density increases with increasing fluence and decrease again at higher fluence which shows saturation. There is however a threshold at which below it the particles are barely visible. For example the threshold for YBCO is about 0.9 J/cm^2 when a XeCL 308 nm excimer laser with 20 ns pulses is used [33]. Crystalline quality of the films improves with increasing fluence. The increased energy cause an increase in plasma density and enhancement of mobility of the deposited atoms on substrate surface and this result in better orientation and thus improved crystalinity [34]. The improvement of crystallization with increased laser fluence was also showed by Fang *et al*. [35].

2.9.2. Background gas

The background gas determines the mean free path length, the kinetic energy, the time the particles takes inside the plume and ultimately the size of the particles adhering onto the substrate[36]. At a pressure of the order of 1 mTorr, the mean free path length is approximately 5 cm. At a higher pressure of about 100 mTorr the path length becomes 0.05 cm. The increased collisions decreases the kinetic energies of the particles, slowing them down, increasing their stay time in the plume as they move slower and this gives them enough time to nucleate and grow into bigger nano-particles. An increase in the gas pressure would then increase the particle sizes as a result of increased collisions between the gas particles and the particles in the plume [37, 38, 39]. Scharf and Krebs [38] studied the influence of inert gas pressure on deposition rate during PLD. They reported that under ultrahigh vacuum, resputtering from the film surface occurs due to the presence of energetic particles in the plasma plume. With increasing gas

pressure, a reduction of the particle energy is accompanied with a decrease of resputtering and a rise in the deposition rate. At higher gas pressures, scattering of ablated material out of the deposition path between target and substrate was observed, and this lead to a decrease in the deposition rate. The maximum deposition rate was obtained in a He pressure of about 300 mTorr.

2.9.3. Substrate temperature

The substrate temperature also plays a significant role during PLD and influences the kinetic energies of the particles once on the substrate surface which leads to better crystalinity. Kang *et al*. [40] and Cho *et al*. [41] reported this during investigating the effect of substrate temperature on structural, optical and electrical properties of ZnO thin films deposited by PLD and the investigation of optical properties of sol-gel derived Y_2O_3:Eu^{3+} thin film phosphors for display applications respectively. The substrate temperature not only affects the crystallinity but it can also influence the thin film composition. XRD results obtained by Kang *et al*. [40] showed a constraint in the growth of the crystal due to low atomic mobility at a deposited temperature of 100 °C. An increase to 500 °C supplied the atoms on the substrate surface with more thermal energy and thus increased their surface mobility that lead to better crystallization. However at too high temperatures such as 700 °C, decrease in the crystallinity of the thin films was observed and it was due to desorption and dissociation of atoms.

2.9. References

[1] Einstein.sc.mahidol.ac.th/~jose/pdf/photoluminescence.pdf [Accessed 28 August 2013]

[2] www.physik.unibas.ch/Praktikum/VPII/Fluoreszen/Fluorescence_and_Phosphorescence.pdf [Accessed 28 August 2013]

[3] H. H. Jaffe, Albert L. Miller, J. Chem. Educ. 43 (9)(1966) 469

[4] IUPAC, Compendium of Chemical Terminology, 2nd ed. (the "Gold Book") (1997). Online corrected version: (2006–) "Intersystem crossing"

[5] http://www.osti.gov/bridge/servlets/purl/948078-pS51LA/948078.pdf [Acccessed 5 September 2013]

[6] P. Schlotter, R. Schmidt, J. Schneider, Appl. Phys. A 64 (1997) 417

Min-Lee, W.L. McLean, M. Croft, Appl. Phys. Lett. 51 (1987) 619

[7] S.W. Allison, G.T. Gillies, A.J. Rondinone, M.R. Cates, Nanotechnology. 14 (2003) 859

[8] H. Bechtel, P. Schmidt, W. Busselt, S. Baby, Schreinemacher Philips Research Europe Aachen, D-52066 Aachen, Germany; ABSTRACT A new phosphor technology for phosphor converted light-emitting.

[9] S.W. Allison, G.T. Gillies, Rev Sci Inst. 68(7) (1997) 261

[10] G. Xia, S. Zhou, J. Zhang, J. Xu, J Cryst Growth. 279(2005)357

[11] J. Tous. K. Blazek, L. Pina, B. Sopko, Radiat. Meas. 42(4-5) (2007) 925

[12] S.W. Allison, G.T. Gillies, A.J. Rondinone , M.R. Cates, Nanotechnology. 14 (2003) 859

[13] R. Hansel, S. Allison and G. Walker, J. Mater Sci. 45 (2010) 146-150

[14] J. Kuo-W. Chen, The electrical and optical properties of doped Yttrium, Aluminum Garnets, PhD thesis, University of California, Berkeley (1987) p 77

[15] F. Xin, S. Zhao, S. Xu, G. Jia, D. Deng, H. Wang, L. Huang, J. Rare Earths. 30(1) (2012) 21-24

[16] Y. Wang, J. Zhang, D. Hou, H. Liang, P. Dorenbos, S. Sun, Y. Tao, Opt. Mat. 34 (2012) 1214–1218

[17] R. Hua, B. Lei, D. Xie, C. Shi, J. Sol. Stat. Chem. 175 (2003) 284

[18] T.A. Obrien, P.D. Rack, P.H. Holloway, M.C. Zerner, J. Lumin. 78 (1998) 245

[19] E. Coetsee, J.J. Terblans, O.M. Ntwaeaborwa, H.C. Swart, Physica B: Physics of Condensed Matter. 404 (22) (2009) 4426 - 4430

[20] L. van Pieterson, M.F. Reid, R. T. Wegh, S. Soverna, A. Meijerink, Phys. Rev. B. 65 (2002) 045113

[21] J.Jennifer, L. Wu, G. Gundiah, A.K. Cheetham, Chem. Phys. Let. 441 (2007) 250-254

[22] S.T.S. Dlamini, H.C. Swart, O.M. Ntwaeaborwa, Sol. State Sci. 23 (2013) 65-71

[23] R.D. Shannon, Acta Cryst A. 32 (1976) 751

[24] K. Brandenburg, DIAMOND-3.0e, Visual crystal structure information System, Crystal impact distribution, Bonn, Germany, 1998

[25] H.C. Swart, E Coetzee, J.J. Terblans, O.M. Ntwaeaborwa, P.D. Nsimama, F.B. Dejene and J.J. Dolo. 101(4) (2010) 633-638

[26] K. T. Hillie, C. Curren and H. C. Swart, Appl. Surf. Sci. 177 (2001) 73

[27] L. Chen, Particles generated by pulsed laser ablation, in: CHRISEY, D.B., HULBER, G.K., (Eds.), Pulsed Laser Deposition of Thin Films, John Wiley & Sons, Inc, New York, 1994, p. 184

[28] K. T. Hillie, H. C. Swart, Appl. Surf. Sci. 183 (2001) 304

[29] E. Coetsee, H.C. Swart, J.J. Terblans ,Vac. Sci. Technol. A 25(2007) 4

[30] D. Dijkkamp, T. Venkatesan, X.D. Wu, S.A. Shaheen, N.Y.H. Jisrawi, Y.H.

[31] I. Ohkubo, Y. Matsumoto, K. Ueno, T. Chikyow, M. Kawasaki, H. Koinuma, J. Crystal Growth. 247 (2003) 105–109

[32] S. Witanachchi, K. Ahmed, P. Sakthivel, P. Mukherjee, Appl. Phys. Lett. 66(1995) 1469

[33] L. Chen, Particles generated by pulsed laser ablation, in D. B. Chrisey, G. K. Hulber (Eds), "Pulsed Laser Deposition of Thin Films", John Wiley & Sons, Inc, New York, (1994) chap. no. 6, p. 167

[34] X. L. Tong, D. S. Jiang, L. Liu, Z. M. Liu, M. Z. Luo, Optics Communications. 270 (2007) 356

[35] L. Fang, M. Shen, J. Crystal Growth. 310 (2008) 3470

[36] A. Matsunawa, S. Katayama, A. Susuki and T. Ariyasu, Trans. J. Welding Res. Inc, 15 (1986) 61

[37] Krebs, M. Weisheit, J. Faupel, E. Suske, T. Scharf, C. Fuhse, M. Stormer, K. Sturm, M. Seibt, H. Kijewski, D. Nelke, E. Panchenko and M. Buback, “Pulsed Laser Deposition (PLD) – a Versatile Thin Film Technique”, B. Kramer, Advances in Solid State Physics, Springer Berlin/Heidelberg, 43 (2003) 101

[38] T. Scharf, H. U. Krebs, Appl. Phys. A. 75 (2002) 551

[39] Y. Shen, N. Xu, W. Hu, X. Xu, J. Sun, Z. Ying and J. Wu, Solid State Electron. 52 (2008) 1833

[40] S. J. Kang, Y. H. Joung, H. H. Shin and Y. S. Yoon, J. Mater. Sci: Mater. Electron, 19 (2003) 1073

[41] J. Y. Cho, K. Ko and Y. R. Do, Thin Solid Films. 515 (2007) 3373

Chapter 3

Research Techniques

3.1. Introduction

A brief account of all the main techniques used is given in this chapter. The commercially obtained $Y_3(Al,Ga)_5O_{12}:Ce^{3+}$ phosphor powder was first characterized. Pulsed laser deposition (PLD) was then used to prepare and deposit the thin films of the phosphor. The films were deposited at different conditions and parameters during PLD. Various techniques were then used to analyse and characterize the films and the powder. Scanning Electron Microscopy (SEM) and Atomic Force Microscopy (AFM) were used for structural and topographical analysis. X-ray Diffraction (XRD) was used for structural properties. Photoluminescence spectroscopy (PL) was used to investigate the luminescence properties. Auger Electron Spectroscopy (AES) was used for elemental composition analysis.

3.2. X-RAY DIFFRACTION (XRD)

In XRD, x-rays primarily interact with electrons in atoms. When a beam of monochromatic X-rays strikes a crystal, the X-rays interact with and are scattered by the atoms in each plane. If the path difference for X-rays reflected by successive planes is a whole number of wavelengths, the X-rays will interfere constructively to produce a strong reflected beam otherwise distractive interference will take place. Bragg's law is the basis of XRD analysis. According to Bragg's law, if the spacing between the reflecting planes is d and the glancing angle of the incident X-ray beam is θ then the path difference of the X-rays reflected by successive planes is $2d \sin\theta$. Hence the condition for diffraction is $n\lambda = 2d \sin\theta$, where n is an integer and λ is the wavelength of the

X-ray. If the atoms are arranged in a periodic fashion, as in crystals, the diffracted X-rays will consist of sharp interference maxima (peaks) with the same symmetry as in the distribution of atoms. Therefore from the diffraction pattern the distribution of atoms in a material can be deduced. X-Ray Diffraction (XRD) data in this study was collected by using a D5000 diffractometer using CuKα radiation of λ = 1.5405 nm in the 2θ range from 10° – 66°, with a counting time of 2 s for each step size of 0.0302°.

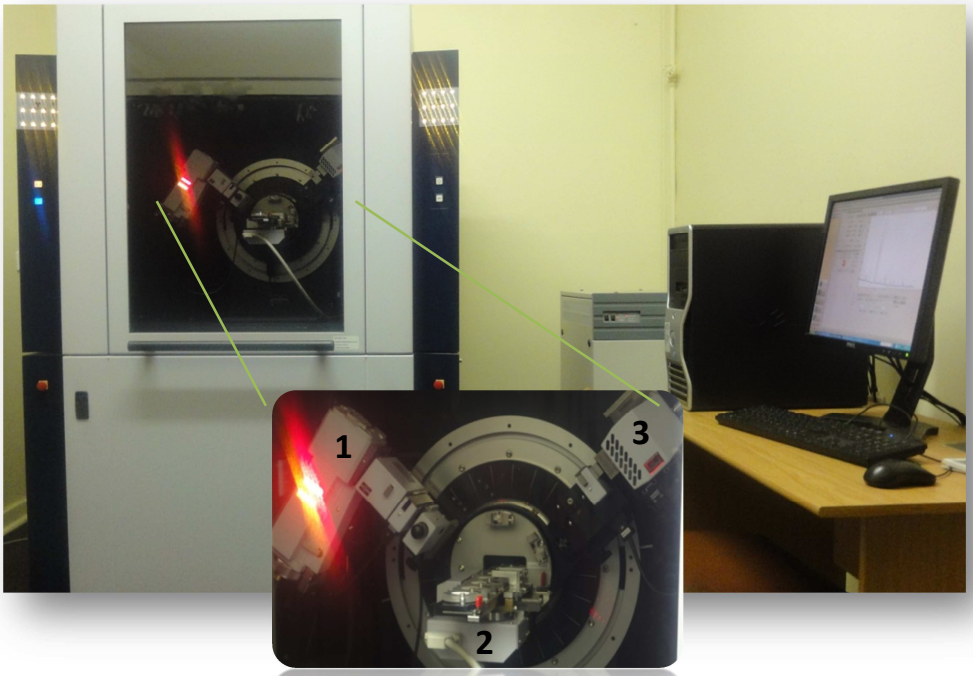

Figure 3.1: The XRD system (D5000 diffractometer) at the University of the Free State, Bloemfontein, South Africa. The zoomed part shows the X-ray source (1), the sample holder (2) and the detector (3).

3.3. SCANNING ELECTRON MICROSCOPY (SEM)

Scanning electron microscopy (SEM) is a method for high-resolution imaging of surfaces. It uses a beam of high-energy electrons (typical range: 5-35keV) to generate variety of signals at the

surface of solid specimens. These signals derived from electron-sample interactions reveal information about the sample including external morphology and orientation of materials making up the sample. The electron beam is produced at the top of the microscope by an electron gun. It then follows a vertical path through the microscope, which is held within a vacuum. The beam travels through electromagnetic fields and lenses, which focus the beam down toward the sample. The electron beam is scanned over the sample. The incident electrons cause electrons to be emitted from the sample, the interaction happens as illustrated in figure 3.2. Around the sample, detectors sense the different signals generated by the electron beam. The most important signals that are detected and analyzed by computer software are secondary and backscattered electrons. Secondary electrons give topographic contrast, which is topographic information about the surface of the sample. Backscattered electrons gives compositional contrast, which is information about the composition of the sample: heavier elements appear brighter on the image on the screen. In most applications, data are collected over a selected area of the surface of the sample, and a 2-dimensional image is generated that displays spatial variations in these properties. Areas ranging from approximately 1 cm to 5 microns in width can be imaged in a scanning mode using conventional SEM techniques (magnification ranging from 20X to approximately 30,000X, spatial resolution of 50 to 100 nm). The SEM is also capable of performing analyses of selected point locations on the sample; this approach is especially useful in qualitatively or semi-quantitatively determining chemical compositions, crystalline structure, and crystal orientations. SEM images of the powder were captured using a Shimadzu Superscan SSX-500 SEM system.

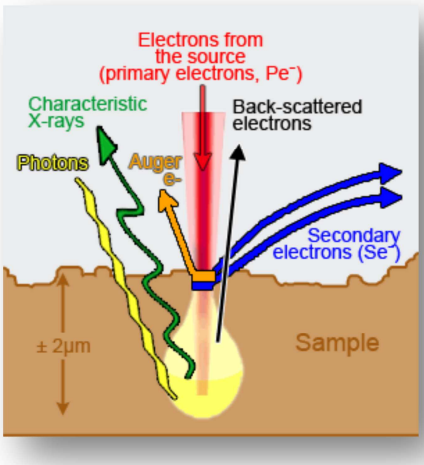

Figure 3.2: Electron-sample interaction [1].

3.4. ATOMIC FORCE MICROSCOPY (AFM)

Atomic Force Microscopy (AFM) is a form of scanning probe microscopy (SPM). It uses a small probe that is scanned across the sample to obtain information about the sample's surface. The information gathered from the interaction of the probe with the surface can be physical topography or measurements of the material's physical, magnetic, or chemical properties. These data are collected as the probe is scanned in a raster pattern across the sample to form a map of the measured property relative to the X-Y position.

The AFM probe has a very sharp tip, often less than 10 nm diameter, at the end of a small cantilever beam. The probe is attached to a piezoelectric scanner tube, which scans the probe across a selected area of the sample surface. Interatomic forces between the probe tip and the sample surface cause the cantilever to deflect as the sample's surface topography (or other properties) changes. A laser light is focused on the back of the cantilever and the position of the reflected beam is monitored by a position sensitive detector (PSD). The PSD measures the position of the laser light spot in 2-dimensions on a sensor surface. The information is fed back

to a computer, which generates a map of topography and/or other properties of interest. Areas as large as about 100 μm square to less than 100 nm square can be imaged [2]. The AFM operates in three modes, the contact, non-contact and tapping mode [3]. AFM was used to obtain micrographs of the surface using the Shimadzu SPM – 9600 model. The root mean square (RMS) values were obtained with the commercial software coming with the AFM system.

3.5. PHOTOLUMINESCENSE SPECTROSCOPY (PL)

Photoluminescence spectroscopy (PL) is a contactless, nondestructive method of physically exploring the electronic structure of materials. A source of excitation is directed onto a sample (the source of excitation can be the UV light, electron beam or laser), where it is absorbed and imparts excess energy into the material. In a case of UV light the process is called photo-excitation. One way this excess energy can be dissipated by the sample is through the emission of light, or luminescence. In the case of photo-excitation, this luminescence is called photoluminescence. The intensity and spectral content of this photoluminescence is a direct measure of various important material properties. Photo-excitation causes electrons within the material to move into permissible excited states. When these electrons return to their equilibrium states, the excess energy is released and may include the emission of light (a radiative process) or may not (a non-radiative process). The energy of the emitted light (photoluminescence) relates to the difference in energy levels between the two electron states involved in the transition between the excited state and the equilibrium state. The quantity of the emitted light is related to the relative contribution of the radiative process. PL excitation and emission spectra were recorded using a Cary Eclipse fluorescence spectrophotometer (Model: LS 55) at room temperature using a 140 W monochromatized Xenon flash lamp as an excitation source. The slit (aperture) used between the lamp and the sample was adjust in such a way that a large part of the sample was

exposed to the excitation beam to make sure an average emission intensity was obtained over a large area.

3.6. AUGER ELECTRON SPECTROSCOPY (AES)

Auger Electron Spectroscopy (AES, Auger) is a surface-sensitive analytical technique that utilizes a high energy electron beam as an excitation source. Auger Electron Spectroscopy provides information about the chemical composition of the outermost material comprising a solid surface or interface. The principal advantages of AES over other surface analysis methods are excellent spatial resolution (< 1 μm), surface sensitivity (≈20 Å), and detection of light elements. AES uses a primary electron beam (0.5 - 30 keV) to excite the sample surface. During the Auger process, the high-energy primary electron hits and ejects a core level electron leading to an ionized atom. For this atom to reorganize itself to a lower energy state, an electron from the higher level will drop to the lower level to fill the vacancy caused by the ejected electron. The excess energy released in this transition is either emitted as a photon or given to another electron in the higher level. If the energy is sufficient, this electron can be ejected from the surface and detected as an Auger secondary electron. Due to the specific energy levels involved in the transition and the energy of the detected Auger electron, the atom from which the electron was ejected can be identified. With the use of an incorporated ion gun into the vacuum system, AES can also be utilized for depth profiling. As the ion gun etches away the material, the electron probe focused on the same spot can give information about the changes in element concentration with sputter depth.

AES's depth profiles and AES survey test of the surface before and after depth profile where performed using a PHI 700 Scanning Auger Nanoprobe. AES surveys were done with a 25 kV

10 nA electron beam. Depth profiles were sputtered with a 2 kV, 2 µA ion beam, at 1×1 mm raster area with sputter rate of 27 nm per min.

3.7. RUTHERFORD BACKSCATTERING SPECTROSCOPY (RBS)

Rutherford Backscattering Spectroscopy (RBS) is a widely used nuclear method for the near surface layer analysis of solids. A target is bombarded with He^+ ions at an energy in the MeV-range (typically 0.5 – 4 MeV), and the energy of the backscattered projectiles is recorded with an energy sensitive detector, typically a solid state detector. The energy detected is characteristic of the mass and depth of the target atom. RBS allows the quantitative determination of the composition of a material and depth profiling of individual elements.

RBS was used to collect composition and thickness information of the thin films. The films were irradiated with 2 Me He^+ ions.

3.8. PULSED LASER DEPOSITION (PLD) TECHNIQUE

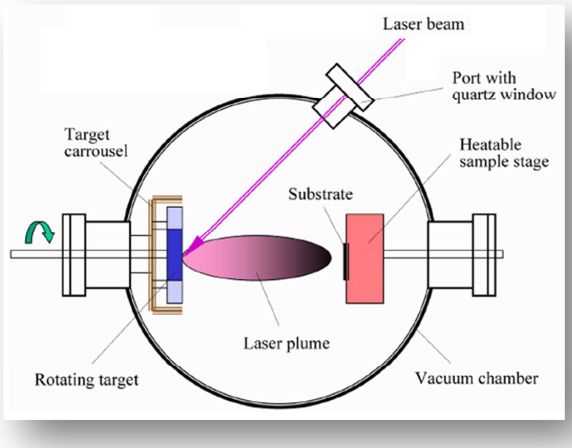

Figure 3.3: Schematic diagram for the PLD set up and process. [4]

The main idea behind the PLD technique is to use pulses from a high-power laser, e.g., Nd: YAG, an excimer or another similar laser, in order to evaporate a small amount of matter from a solid target. Figure 3.3 shows a schematic diagram for the PLD process. The laser is focused and absorbed at the target surface in a small volume. A supersonic jet of particles is ejected normal to the surface of the target. The cloud of particles then absorbs a large amount of the energy from the laser beam producing an expansion of hot plasma or plume through the deposition chamber. Then these ablated species condense on the substrate placed opposite to the target forming a thin film. The films can be produced in high vacuum, but typically the films are produced in a reactive background gas, such as oxygen (used for the production of oxide films) or nitrogen (used for nitride films). Also an inactive background gas such as argon is frequently used. In actuality the interaction of the laser beam with the target surface and the growth of the film are far more complicated processes than what is explained above. In fact the principle of PLD is a

very complex physical phenomenon despite the simplicity of the basic setup of the PLD system. Below, a general overview of the different process that takes place during PLD is discussed.

The process of PLD can generally be categorized into the following stages:

3.8.1. Interaction of the laser with the target material and the ablation of the plasma plume

The laser light is absorbed in the solid material, and atoms as well as ions and electrons are ejected from the solid material. The magnitude of the ablation yield is determined by the cohesive energy, i.e. the energy required to release an atom from a solid. The laser–solid interaction mechanisms may depend on the laser wavelength. The most important effect of the laser's wavelength is its determination of the penetration depth. Most of the energy should be absorbed in a very shallow layer near the surface of the solid to avoid subsurface boiling, which can lead to a large number of particulates at the film surface. The cloud of particles then absorbs

a large amount of the energy from the laser beam producing an expansion of hot plasma or plume through the deposition chamber. The plume expands away from the solid target much like the rocket exhaust from jet nozzles, with strongly forward-directed supersonic velocity distribution. The plume consists of several types of particles: neutral atoms, electrons, ions and even clusters of different compounds of the target elements

3.8.2. The plasma plume dynamics

The film growth can be done with the chamber in vacuum or in the presence of a background gas. In case of a background gas present in the chamber, the initial high pressure drives the ablation plume towards the background gas which acts as a piston. The plume slows down and is confined in the background gas. Eventually, the atoms diffuse out of the plume and migrate to the substrate or the chamber walls [5–8]. The mass of the plume is important for the propagation

dynamics. The total mass of the plume plays a role for the slowing-down of the plume, but the individual masses from a multicomponent plume only influence the behavior as a part of the total plume. The mass density of the displaced gas is an important parameter as well [9, 10]. The angular distribution of the plume atoms is influenced by the mass density of the background gas as well. For heavy gases the broadening of the angular distribution occurs at a much lower pressure than for light gases [6, 11]. This reflects the fact that light atoms in a heavy gas are scattered much more than heavy atoms in a heavy gas. It is generally assumed that some degree of thermalization (i.e. having equal lateral and forward velocities) needs to occur in order to obtain good film growth and to avoid re-sputtering of the growing film by the most energetic ions in the plume [12]. This is the reason why a background gas is always preferred over vacuum condition in the chamber.

3.8.3. Deposition, nucleation and growth of the film on the substrate surface:

The growth of a film on a substrate surface is in itself a very complicated process [13]. Arriving atoms (or molecules) may stick to the surface at the point of impact, but atoms from a laser ablation plume typically possess sufficient kinetic energy to diffuse some distance on the surface, until stable, energetically favorable bonds with the other film atoms or substrate atoms have been established. A necessary condition for stoichiometry in the film is that atoms of all components are available in the desirable ratio at the growth points. The primary processes which take place on a microscopic scale are (i) atom/ion reflection on the surface, (ii) sputtering of film atoms by the ablated atoms and (iii) implantation of arriving atoms. Sputtering of the growing film leads to an enrichment of the least volatile component (often the heaviest component) in the film. Sputtering by and implantation of the plume atoms usually lead to an enrichment of the heaviest

atoms at the surface therefore the bombardment of the surface by ablated ions can radically change the stoichiometry. One parameter is the laser fluence, by which the energies of the ablated particles are controlled. The effects of reflection, sputtering and implantation can be reduced at the moderate fluence which actually often is used in PLD thus leading to the same stoichiometry between the films and the target.

An Nd:YAG 266 nm laser was used in this study to deposit the phosphor target. The laser fluency was kept at 0.78 J/cm^2 with a 10 Hz frequency for all the depositions. Silicon (100) wafers were used as substrates. They were cut into approximately 2 cm by 2 cm pieces and cleaned in an acetone ultrasonic bath for 15 minutes. The phosphor target and one silicon piece at a time were inserted into the PLD chamber. The target to substrate distance was kept at 6 cm. To investigate the effect of the number of pulses from the laser on the growth of the $Y_3(Al,Ga)_5O_{12}:Ce^{3+}$ films, the chamber was backfilled with O_2 gas at 10 mtorr pressure and

ablation was done while the number of pulses from the Nd:YAG laser was varied from 10 000, 20 000 and 40 000 pulses with the substrate temperature kept constant at 300°C. Then to investigate the effect of substrate temperature, the number of pulses were kept constant at 20 000 pulses and the ablation was done at the substrate temperatures of 22°C (Room Temperature) 100°C, 300°C and 500°C for chamber atmospheres of 10 mtorr O_2 and Ar, respectively. For the investigation of the effects of PLD chamber atmospheres, the substrate temperature and the number of pulses were kept constant at 300°C and 20 000 pulses respectively. Ablation was first done in the chamber with a vacuum pressure of 10^{-6} mbar, then in O_2 and Ar atmospheres at pressures of 5, 10 and 20 mtorr, respectively for both gases.

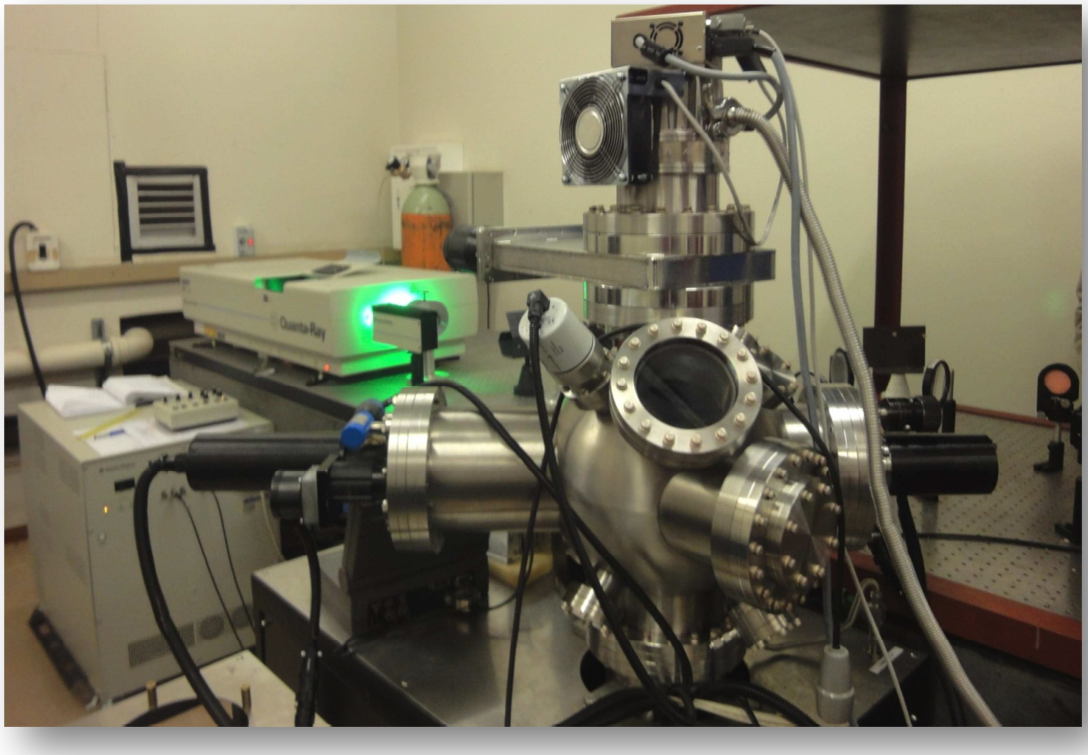

Figure3.4: The Pulsed Laser Deposition (PLD) Machine at the National Laser Centre (NLC, CSIR), Pretoria, South Africa.

3.9. References.

[1] http://www.vcbio.science.ru.nl/en/fesem/info/principe/ [Accessed 14 August 2013]

[2] http://mee-inc.com/afm.html [accessed 19 August 2013]

[3] R. Fung, S. Huang, J. Vib. Acoust. 123 (2001) 502

[4] http://titan.physx.u-szeged.hu/~lamilab/plden.htm [accessed 19 August 2013]

[5] S. Amoruso, R. Bruzzese, N. Spinelli, R. Velotta, M. Vitiello, X. Wang, Phys. Rev. B 67 (2003) 224503

[6] S. Amoruso, B. Toftmann, J. Schou, Phys. Rev. E. 69 (2004) 056403

[7] H.C. Lee, D.E. Zeitoun, J.D. Parisse, M. Sentis, W. Marine, Phys. Rev. E. 62 (2000) 4152

[8] Y. Nakata, W.K.A. Kumuduni, T. Okada, M. Maeda, Appl. Phys. Lett. 64 (1994) 2599

[9] S. Amoruso, J. Schou, J.G. Lunney, Appl. Phys. A. 92 (2008) 907

[10] R.K. Singh, J. Narayan, Phys. Rev. B. 41 (1990) 8843

[11] S. Amoruso, B. Toftmann, J. Schou, Appl. Surf. Sci. 248 (2005) 323

[12] S.K. Hau, K.H. Wong, P.W. Chan, C.L. Choy, Intrinsic resputtering in pulsed-laser deposition of lead-zirconate-titanate thin films, Appl. Phys. Lett. 66 (1995) 245

[13] D.L. Smith, Thin Film Deposition—Principles and Practice, McGraw-Hill, New York, 1994p.119

Chapter 4

Morphological and luminescent properties of $Y_3(Al,Ga)_5O_{12}:Ce^{3+}$ powder phosphor.

4.1. Introduction

Cerium-doped yttrium aluminum garnet ($Y_3Al_5O_{12}:Ce^{3+}$ or YAG:Ce) is used in several applications such as solid state lighting and displays. The Ce^{3+} ion is responsible for a nanosecond decay time and an intense emission at a visible wavelength range. Most phosphors have been developed for the use in fluorescent tubes or compact fluorescent lamps (CFLs) that use UV radiation, but yet they have not been optimized for the use in light emitting diodes (LEDs) that emit in the visible spectrum range. The first basic commercially available white LED is based on an InGaN chip emitting blue light at a wavelength of 460 nm that is coated with a YAG:Ce phosphor layer that converted some of the blue light into yellow light which is combined to a rather cool white light [1]. This is good for many applications (e.g., displays and lighting in cars), but the quality of light is not good enough for home lighting, for which a warmer white light containing some red light is desirable. Some of the Al in the YAG:Ce^{3+}, is often replaced with Ga^{3+} to form $Y_3(Al,Ga)_5O_{12}:Ce^{3+}$ due to the similarity in cation size to get the red light component in LEDs [2]. Knowing properties of this phosphor in detail could lead to the application of this phosphor in manufacturing of LEDs for home lighting. In this work the $Y_3(AlGa)_5O_{12}:Ce^{3+}$ powder phosphor is characterized with different techniques.

4.2. Experimental

In this study a commercial $Y_3(Al,Ga)_5O_{12}:Ce^{3+}$ powder phosphor was obtained from Phosphor Technology with CIE coordinates: (x= 0.306, y=0.521) [3]. By using X-ray Diffraction (XRD) the powder was characterized for its phase purity and crystalinity. The D5000 X-ray diffractometer was used to carry out the XRD analysis. Scanning electron microscope (SEM) images of the powder were captured using a Shimadzu Superscan SSX-500 SEM system. Photoluminescence (PL) properties of the phosphor were recorded using the Carry eclipse spectrophotometer at room temperature with a monochromatized Xenon flash lamp as an excitation source. The UV-VUV excitation and emission spectra of the $Y_3(Al,Ga)_5O_{12}:Ce^{3+}$ were recorded between 100 to 330 nm and 252 nm, respectively, by using the UV-VUV synchrotron radiation facility at the SUPERLUMI beamline I of HASYLAB (Hamburger Synchrotron strahlungslabor) at DESY (Deutsches Elektronen-Synchrotron, Hamburg, Germany) [4]. The spectra were recorded at room temperature. The setup consisted of a 2-m McPherson type primary (excitation) monochromator with a resolution up to 0.02 nm. The UV-VUV excitation spectra were corrected for the variation in the incident flux of the excitation beam using the excitation spectrum of sodium salicylate as a standard.

4.3. Results

The XRD pattern of $Y_3(Al,Ga)_5O_{12}:Ce^{3+}$ reveals a cubic polycrystalline phase with the main peak centered at $2\theta = 32.9°$. The pattern corresponds to the cubic phase in the reference data ICSD No 029250. Using Scherrer's equation and the XRD peaks, the average crystal size of the phosphor was estimated to be around 80 nm.

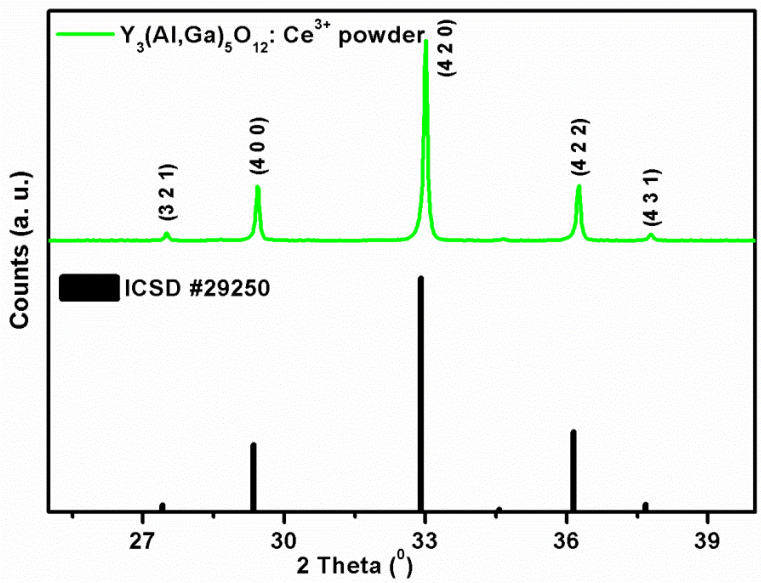

Figure 4.1: XRD pattern of phosphor and the ISCD reference profile.

The microstructure of $Y_3(Al,Ga)_5O_{12}:Ce^{3+}$ was characterized from SEM micrographs. As shown in the images in figure 4.2, $Y_3(Al,Ga)_5O_{12}:Ce^{3+}$ phosphor was made up of an agglomeration of faceted spherical particles. The particle sizes were ranging from 0.5 µm to 1.4 µm.

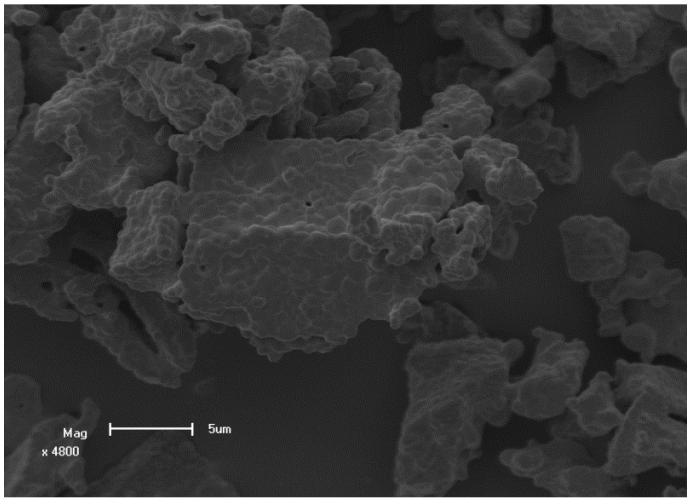

Figure 4.2: SEM images of the commercially obtained $Y_3(AlGa)_5O_{12}:Ce^{3+}$ phosphor.

The PL excitation and emission spectra of the $Y_3(Al,Ga)_5O_{12}:Ce^{3+}$ phosphor are shown in figure 4.3. The excitation peaks are due to the 4f to 5d transitions of electrons in the Ce^{3+} ion and the emission spectra is attributed to the de-excitation of these electron from the lowest 5d level to the field split 4f levels. Blue-shifts in the PL emission spectra are an indication of structural changes caused by the substitution of Al with Ga in the phosphor host. Table 4.1 shows emission data with different concentrations of Ga in the Ce^{3+} doped garnets [2]. From the table and the PL spectra in figure 4.3 it can be estimated that there is roughly 60% Ga and 40% Al in the $Y_3(Al,Ga)_5O_{12}:Ce^{3+}$ crystal structure and also table 4.1 shows the shift in the emission and excitation wavelength from 504 nm and 422 nm to 540 nm and 457 nm respectively as Al is substituted for Ga within the phosphor host. When Al^{3+} is substituted with Ga^{3+}, the Ga-O bonds re-adjust due to the difference in atomic radius of Ga^{3+} which is larger than Al^{3+}. The schematics of the relative arrangement of Y, O, Al and Ga were drawn using the diamond crystal software [5] and are shown in figure 2.3. The Y/Ce ions are surrounded by O^{2-} ions in the dodecahedral arrangement. The Al^{3+} and Ga^{3+} are surrounded by O^{2-} ions in a tetrahedral and octahedral arrangement. Ultimately, the substitution of Ga into the YAG lattice resulting in a decompression of oxygen atoms directly coordinated to the Ce^{3+} atom and the structure becomes more cubic. This change in structure directly affects the 5d orbitals of the Ce^{3+} and likewise the PL characteristics [2].

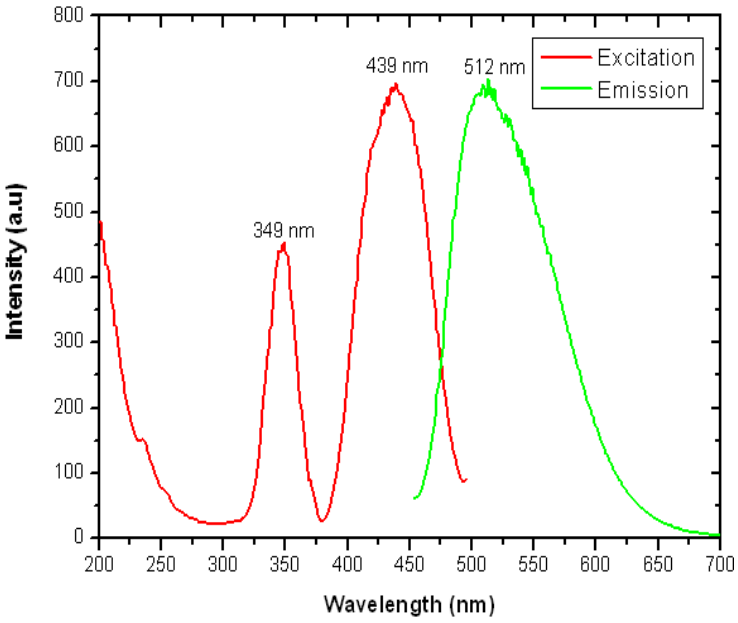

Figure 4.3: PL spectra of $Y_3(Al,Ga)O_{12}:Ce^{3+}$ with the emission spectra monitored at the excitation wavelength of 439 nm.

Table 4.1: Spectroscopic and structural properties of Ce^{3+} doped garnets [2]

Host	λex(nm)	λem(nm)
$Y_3Al_5O_{12}$	457	540
$Y_3Al_4GaO_{12}$	447	527
$Y_3Al_3Ga_2O_{12}$	440	523
$Y_3Al_2Ga_3O_{12}$	430	512
$Y_3AlGa_4O_{12}$	422	504

Figure 4.4 shows the relative placement of the 5d orbitals in $Y_3Al_5O_{12}:Ce^{3+}$ (YAG: Ce) and $Y_3(Al,Ga)_5O_{12}:Ce^{3+}$ (YAGG:Ce). Electrons are excited to the E" state of the 5d orbital and are emitted from the E' state. The splitting of the E" and E' states is determined by the crystal field around the Ce^{3+} atom. In unsubstituted YAG, the oxygen atoms around the Ce^{3+} atom are highly compressed and form a non-cubic structure. The splitting of the E" and E' states increases as the oxygen atoms are further distorted from the cubic structure. As Ga is substituted into YAG, oxygen atoms surrounding the Ce^{3+} atom are decompressed and form a cubic structure. As a result, the splitting between the E" and E' states decreases with the Ga content. Consequently, the samples with Ga have noticeably shorter emission wavelengths (higher energy) [6].

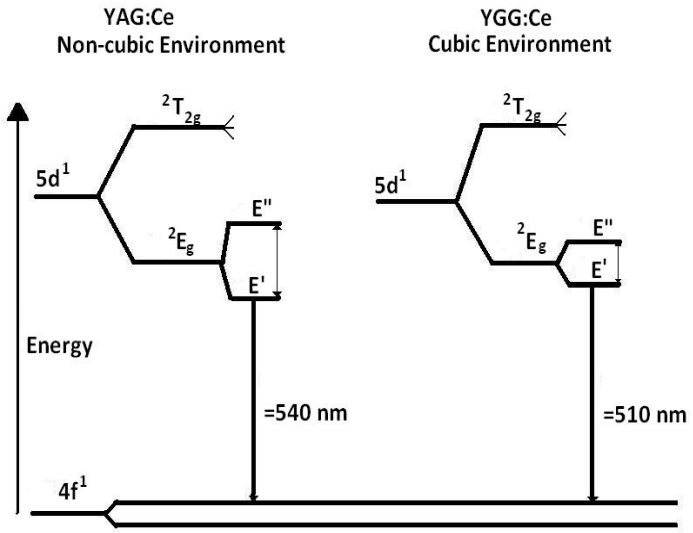

Figure 4.4: Energy level diagram for YAG: Ce and YAGG:Ce (not drawn to scale)[6]

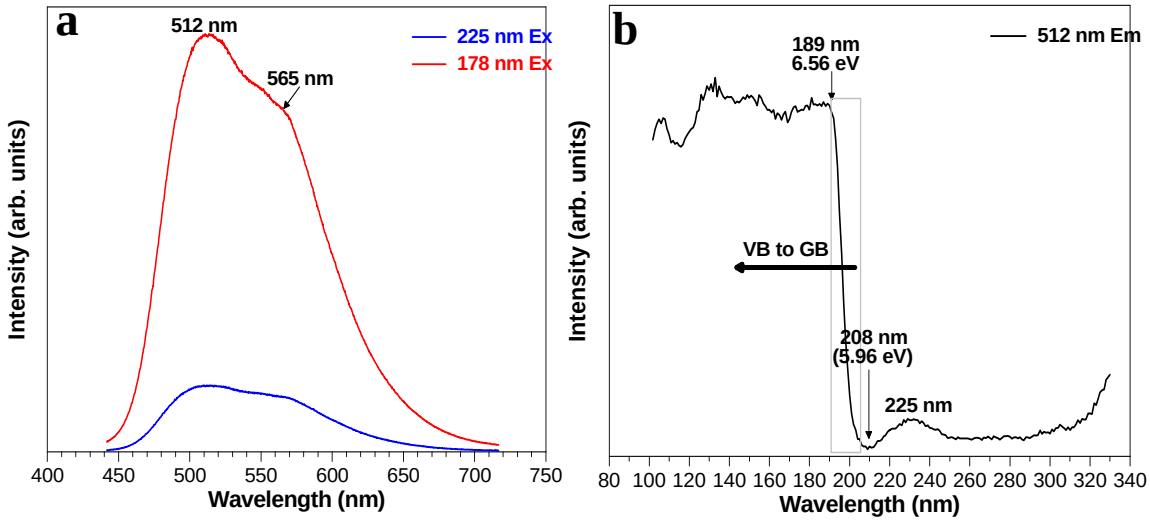

Figure 4.5: (a) The emission spectra of the $Y_3(Al,Ga)_5O_{12}:Ce^{3+}$ phosphor monitored at excitation wavelengths of 225 nm and 178 nm. (b) Excitation spectra of the $Y_3(Al,Ga)_5O_{12}:Ce^{3+}$ phosphor measured at an emission wavelength of 512 nm.

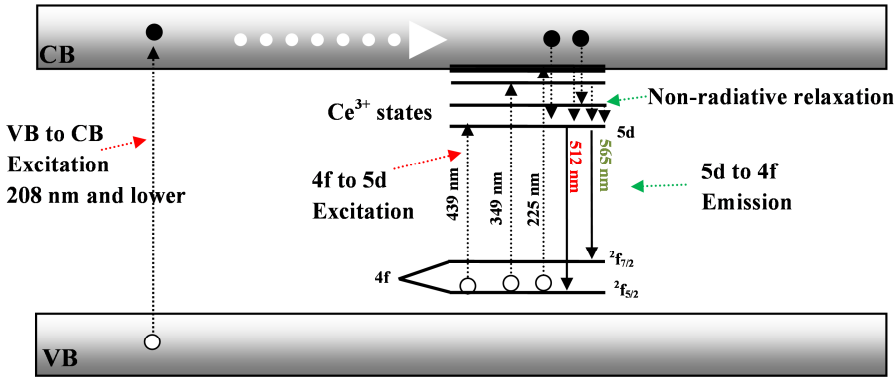

Figure 4.6: The energy diagram of the $Y_3(Al,Ga)_5O_{12}:Ce^{3+}$ phosphor showing the excitation and emission as compiled from the emission and excitation spectra.

The excitation and emission spectra of the $Y_3(Al,Ga)_5O_{12}:Ce^{3+}$ phosphor powder measured with the Cary Eclipse fluorescence spectrophotometer are shown in figure 4.3. Excitation peaks were obtained at 349 nm and 439 nm with a shoulder at 225 nm. An emission peak at 512 nm with a shoulder peak at 565 nm is clear from the emission spectrum. The emission and excitation spectra of $Y_3(Al,Ga)_5O_{12}:Ce^{3+}$ were also obtained under UV-VUV synchrotron radiation, figure 4.5. The excitation spectra of the host were measured at 178 nm and 225 nm at room temperature. Except for the intensity difference the spectra are identical with a broad peak consisting out of two peaks at around 512 and 565 nm. These peaks are from the de-excitation of electrons from the lowest 5d level to the field split 4f ($^2f_{5/2}$ and a $^2f_{7/2}$) levels. Excitation peaks were obtained at 349, 439, 225 and 178 nm, figure 4.3 and 4.5. The last peak that increases from 209 nm up to 189 nm is assigned to the host-related absorption, since many phosphors show host-related absorptions around this spectral range [7]. In this case it is an indication of the band gap absorption of the $Y_3(Al,Ga)_5O_{12}$ between 5.96 eV (208 nm) and 6.56 eV (189 nm). The other

excitation peaks clearly indicate the excitation peaks of the 4f ($^2f_{7/2}$) to 5d levels. It is therefore clear that the Ce^{3+} is excited via the conduction band as well as in the Ce^{3+} ion itself. The PL emission spectrum obtained by Chaoa et al. [8] had a broad emission band that was centered at 545 nm. This emission corresponds to the transition from the 5d excited state to the 4f ground state of the Ce^{3+} ion in the YAG crystal. Their PL excitation spectrum includes two peaks at 340 nm (weak) and 450 nm (strong), which correspond to the characteristic 5d and 4f energy levels. A summary of the energy levels of Ce^{3+} in the $Y_3(Al,Ga)_5O_{12}$ is given in figure 4.6 as obtained and compiled from the measured excitation and emission spectra. The 225 nm excitation and the 209 nm is very close to each other indicating that one of the 5d level must be on the edge of the CB. The Ce^{3+} energy values of the 5d lines obtained from this study compared very well with that obtained by Tomiki et. al.[9]. The values from Tomiki are: 460 nm (2.695 eV); 340 nm (3.643 eV); 266 nm (4.66 eV); 228 nm (5.44 eV) and 204 nm (6.07 eV). In the YAGG:Ce system [10], replacement of Al with the larger Ga ion in the octahedral site increases the lattice constant and decreases the peak excitation/emission wavelength. Excitation and emission values shows that decreasing the lattice constant actually increases the peak emission wavelength while barely affecting the excitation maxima. Kottaisamy et al. [11] found a peak shift to the higher wavelength region which indicated that the lowest 5d level has shifted to a much lower energy level due to co-doping with higher ionic size ions (Gd or La) at the Y site of YAG.

4.4. Conclusions

SEM micrographs showed $Y_3(Al,Ga)_5O_{12}:Ce^{3+}$ phosphor powder that is made up of agglomeration of faceted spherical particles. From the PL emission spectra, it was estimated that there is roughly 60% Ga and 40% Al in the $Y_3(Al,Ga)_5O_{12}:Ce^{3+}$ crystal structure. The excitation peaks indicated that Ce^{3+} is excited via the conduction band as well as in the Ce^{3+} ion itself. The

two emission peaks confirmed the arrangement of the atom in which the Ce^{3+} can only occupy one lattice side position.

4.5. Acknowledgements

For UV-VUV measurements, a special thanks to the synchrotron radiation facility at the SUPERLUMI beam line I of HASYLAB (Hamburger Synchrotron strahlungslabor) at DESY (Deutsches Elektronen-Synchrotron, Hamburg, Germany). The National Research Foundation and the University of the Free State for financial support.

4.6. References

[1] P. Schotter , R. Schmidt, J. Schneider , Appl. Phys. A. 64 (1997) 417-418

[2] J.L. Wu , G. Gundiah, A.K. Cheetham, Chem. Phys. Lett. 441 (2007) 250-254

[3] http://www.phosphor-technology.com/products/crt.htm [Accessed 29 May 2012]

[4] HASYLAB, Beamline I: SUPERLUMI, http://hasylab.desy.de/facilities/doris_iii/beamlines/i_superlumi [Accessed January 2012)

[5] K. Brandenburg, DIAMOND-3.0e, Visual crystal structure information System, Crystal impact distribution, Bonn, Germany, 1998

[6] R. Hansel , S. Allison, G. Walker, J. Mater. Sci. 45 (2010) 146-150

[7] Y. Wang, J. Zhang, D. Hou, H. Liang, P. Dorenbos, S. Sun, Y. Tao, Opt. Mat. 34 (2012) 1214–1218

[8] W.H. Chaoa, R.J. Wub, T.B. Wua, J. of Alloys and Comp. 506 (2010) 98–102

[9] T. Tomiki, H. Akamine, M. Gushiken, Y. Kinjoh, M. Miyazato, T. Miyazato, N. Toyokawa, M. Hiraoka, N. Hirata, Y. Ganaha, and T. Futemma, J. Phys. Soc. Jpn. 60(7) (1991) 2437–2445

[10] J.Jennifer, L. Wu, G. Gundiah, A.K. Cheetham, Chem. Phys. Let. 441 (2007) 250-254

[11] M. Kottaisamy, P. Thiyagarajan, J. Mishra, M.S. Ramachandra Rao, Mat. Res. Bull. 43 (2008)1657–1663

Chapter 5

The effect of different gas atmospheres on the structure, morphology and photoluminescence properties of pulsed laser deposited $Y_3(Al,Ga)_5O_{12}:Ce^{3+}$ nano thin films.

5.1. Introduction

Recently attention has been paid on YAG:Ce because it can be applied to white light emitting diodes (LEDs) as yellow emission phosphors. The Ce^{3+} ion is responsible for nanosecond decay times and an intense yellow-green emission wavelength [1]. Trivalent Ga atoms have been substituted for Al atoms in order to blue-shift the emission wavelength for use in solid-state light applications such as fabrication of white LEDs. The most common method to produce white light with LEDs is the combination of blue InGaN-GaN LEDs with the yellow emitting YAG:Ce phosphor. With a LED emission wavelength of 440 – 470 nm a fraction of the LED emission is absorbed by the YAG:Ce phosphor and down-converted to the well-known broad yellow emission of the phosphor. Not converted blue LED light and the yellow emission are mixed by the phosphor powder layer to obtain white light in a wide range of correlated color temperatures (CCT) from 4000 – 8000 K [2]. It has been shown that YAGG:Ce has characteristics that are suitable for this phosphor to be applied for the fabrication of LEDs [3]. However in literature YAGG:Ce has been studied rather extensively in the powder form but not so much in the thin film form. Particularly thin films that have been prepared by the pulsed laser deposition (PLD) technique did not gain much attention in the past. $Y_{3-x}Al_5O_{12}:Ce_x^{3+}$ (YAG:Ce^{3+}) thin-films were

deposited by a pulsed-laser deposition method on quartz substrates using a solid YAG:Ce target [4]. The as-deposited films were amorphous and annealing the films led to better crystallization. PL spectra of annealed films showed a strong and broad emission band around 570 nm and excitations at 342 and 460 nm, all corresponding to transitions between the $4f^1$ ground level to the $5d^1$ excited levels of Ce^{3+} ion. Thin films offers several advantages due to their good luminescence characteristics, higher image resolution from small grains, better thermal stability and good adhesion to the substrate [3]. The presence of a background gas in a chamber plays an important role in the growth of the thin films during the PLD. There are 3 primary processes which take place on a microscopic scale: the atom/ion reflection on the surface, sputtering of film atoms by the deposited atoms and implantation of arriving atoms [5]. Depending on the pressures inside the chamber, whether the chamber is in vacuum or in the presence of a background gas, one or two of these microscopic processes will be more favored and this significantly affects the growth and properties of the film. In this chapter we report on the morphological and luminescent properties of YAGG:Ce phosphor in the powder form and the thin film prepared by PLD in vacuum and in a background gas of Ar and background gas of O_2 at pressures of 5 mtorr, 10 mtorr and 20 mtorr for both gases. The aim was to identify the PLD gas environment that will produced thin films with a high PL intensity as well as structural properties similar to the YAGG:Ce phosphor in the powder form.

5.2. Experimental Setup

$Y_3(Al,Ga)_5O_{12}:Ce^{3+}$ powder phosphor obtained from Phosphor Technology (UK) with Commission Internationale de l'Eclairage (CIE) chromaticity coordinates: (x= 0.306, y=0.521) and non-uniform particles with median particle size of 2.5 μm were used in this study [6]. The Ga to Al ratio is about 60:40 in the $Y_3(Al,Ga)_5O_{12}:Ce^{3+}$ crystal structure. When Al^{3+} is

substituted with Ga^{3+}, the Ga-O bonds re-adjust due to the difference in atomic radius of Ga^{3+} which is larger than Al^{3+}. The powder was first completely characterized and then pressed without binders to make a pellet which was used as a target for PLD. Silicon (100) wafers were used as substrates. They were cut into approximately 2 cm by 2 cm pieces and cleaned in an acetone ultrasonic bath for 15 minutes. A layer of silicon dioxide was grown on all the films. The phosphor target and one silicon piece at a time were inserted into the PLD chamber. An Nd:YAG 266 nm laser was used to deposit the phosphor target. The laser fluency was kept at 0.78 J/cm^2 with a 10 Hz frequency. The target to substrate distance was kept at 6 cm. The chamber was evacuated to a base pressure of 5×10^{-6} mbar. A film was deposited with a substrate temperature at 300°C at a vacuum pressure of 8×10^{-6} mbar. Then the chamber was backfilled with Ar and then O_2 gas. The ablation was performed at a chamber's pressure of 5 mtorr, 10 mtorr and 20 mtorr for both background gases while the substrate temperature was kept constant at 300°C. Atomic Force Microscopy (AFM) was used to obtain micrographs of the surface using the Shimadzu SPM – 9600 model. The root mean square (RMS) values were obtained with the commercial software coming with the AFM system. Photoluminescence (PL) excitation and emission spectra ware recorded using a Cary Eclipse fluorescence spectrophotometer (Model: LS 55) at room temperature using a 140 W monochromatized Xenon flash lamp as an excitation source. The slit (aperture) used between the lamp and the sample was adjusted in such a way that a large part of the sample was exposed to the excitation beam to make sure an average emission intensity was obtained over a large area of the thin film and possible un-uniformities in the thin films if any are cancelled out if an average emission intensity is obtained. X-Ray Diffraction (XRD) data was collected by using a D5000 diffractometer using CuKα radiation of $\lambda = 1.5405$ nm in the 2θ range from 25° – 40°, with a counting time of 2 s for each step size of 0.0302°.

Rutherford backscattering spectroscopy (RBS) was used to collect composition and thickness information of the thin films. The films were irradiated with 2Me He^{+} ions. Auger Electron Spectroscopy (AES)'s depth profiles and AES survey test of the surface before and after depth profile where performed using a PHI 700 Scanning Auger Nanoprobe. AES surveys were done with a 25 kV 10 nA electron beam. Depth profiles were sputtered with a 2 kV, 2 µA ion beam, at 1×1 mm raster area with sputter rate of 27 nm per min.

5.3. Results

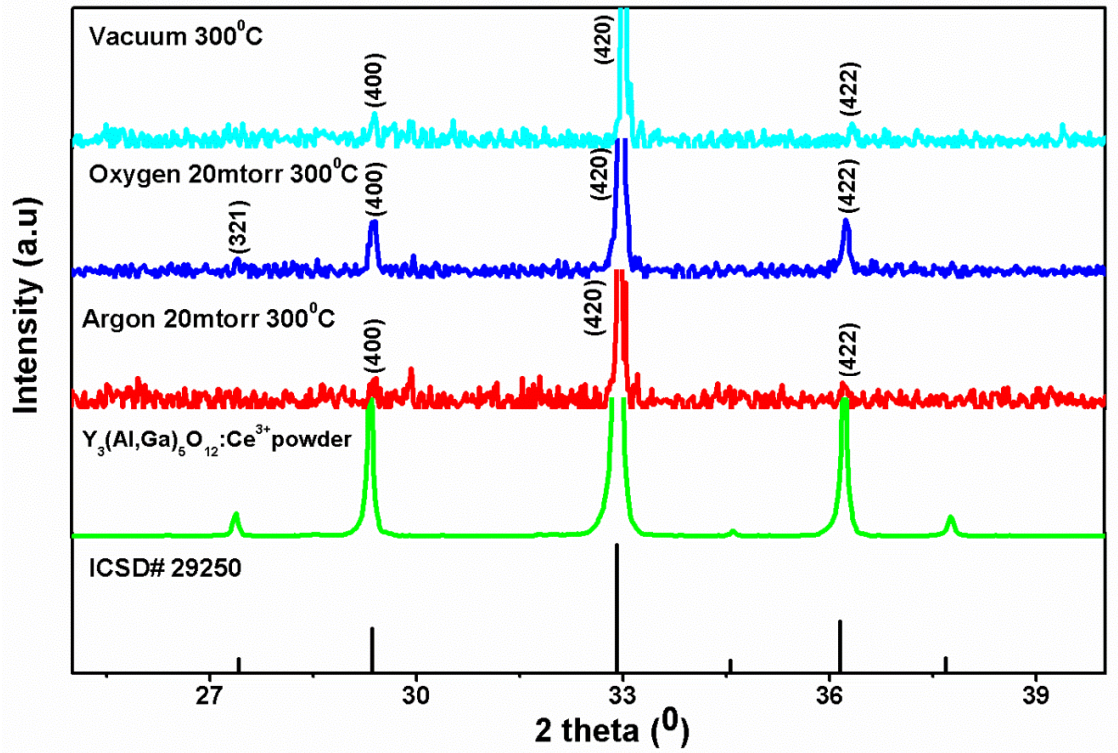

Figure 5.1: XRD spectra of YAGG:Ce powder and films deposited at 300 °C in different gas atmospheres.

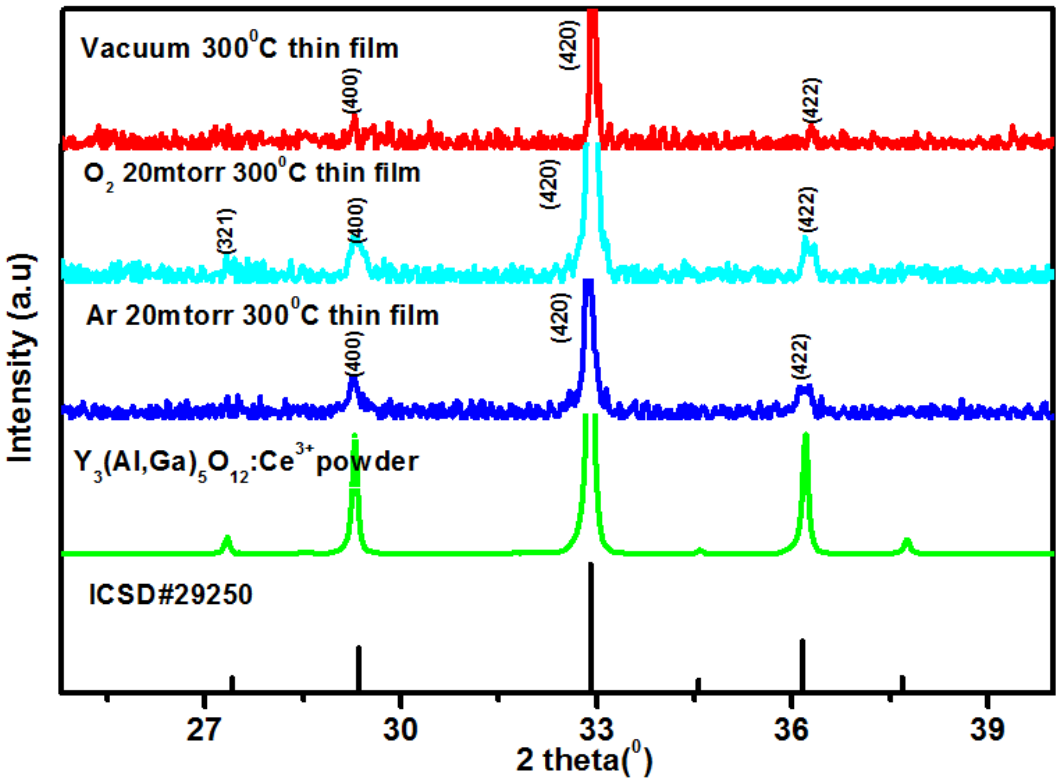

Figure 5.2: XRD spectrum of YAGG:Ce powder and films after annealing at 800 °C in open air.

XRD patterns of the YAGG:Ce phosphor powder and thin films that were deposited in various atmospheres before and after annealing are shown in figure 5.1 and figure 5.2 respectively. The ICSD file number 29250 is also shown. Note that the (420) peaks are cut off in order to enlarge the other reflections. It is clear that crystalline thin films with the same crystal structure as the powder were obtained during the PLD process. The films annealed at 800 °C have only a small effect (improvement) on the crystallinity of the thin film. The XRD peaks of the O_2 are more pronounced which indicate that better crystallinity was obtained in the O_2 atmosphere. The XRD of the other annealed films prepared at the other pressures was similar to the spectra shown.

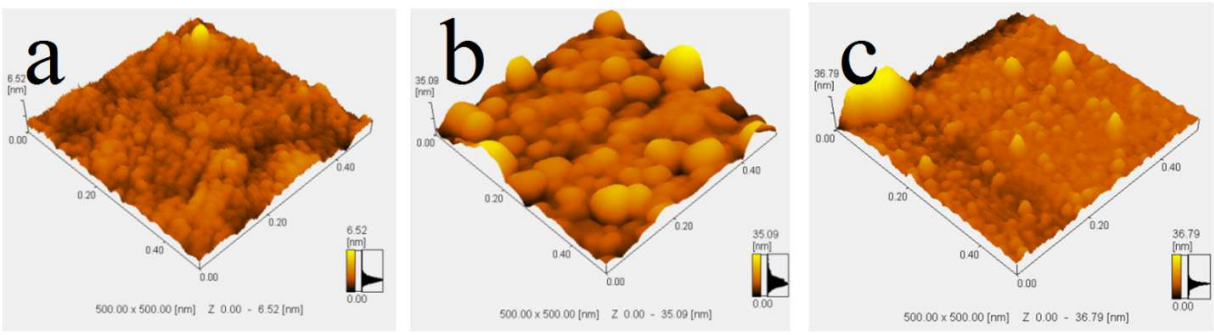

Figure 5.3: AFM micrographs of the film deposited in (a) vacuum (1.6 x 10^{-6} mbar), (b) 20 mtorr Argon and (c) 20 mtorr O_2 at a substrate temperature of 300 $^{\circ}$C

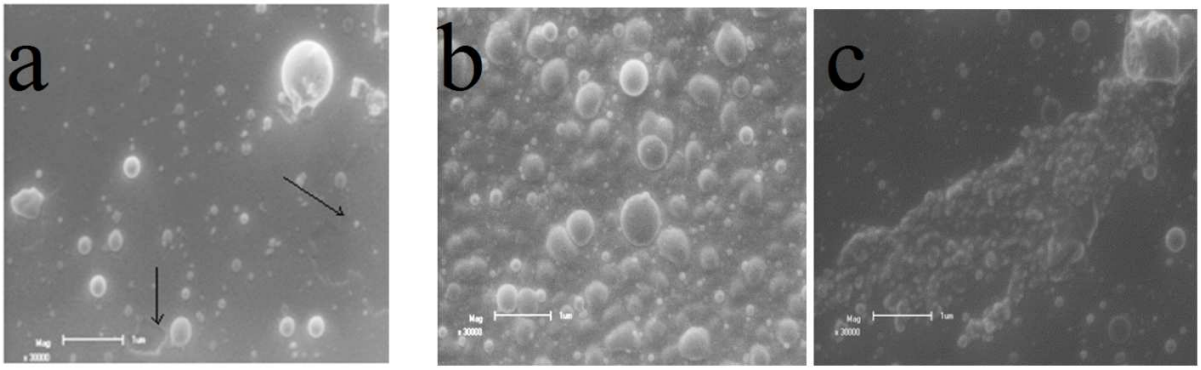

Figure 5.4: SEM micrographs of the films deposited in (a) vacuum (1.6 x 10^{-6} mbar) and (b) 20 mtorr Argon and (c) 20 mtorr O_2 at a substrate temperature of 300 °C

The AFM micrographs obtained, figure 5.3, showed films grown on the silicon substrate under different background atmospheres as indicated. From this AFM images in figure 5.3, it can be seen that films deposited in (a) vacuum (1.6 x 10^{-6} mbar) are smooth and consist of smaller nanoparticles (≈ 30 nm), while the films deposited in (b) 20 mtorr Ar atmosphere, have rough surfaces that consist of much bigger particles (≈ 90 nm). The surfaces of the thin film deposited in (c) 20 mtorr O_2 were also much smoother but much more defined and also consist of nanoparticles(≈ 40 nm). During deposition in vacuum, the plume leaves the target with very high

energy and travels through the chamber to the substrate. In the absence of a background gas, the particles making up the plume (atoms, ions and electrons) are likely to be reflected when they reach the substrate or sputter the already growing film. The SEM image in figure 5.4(a) shows areas on the surface where the material was sputtered or no deposition took place (indicated by the black arrows). Figure 5.4(b) shows a SEM image of a film deposited in an Ar and (c) O_2 atmosphere of 20 mtorr. During a PLD experiment with the pulse of a nanosecond duration the laser energy is initially absorbed by the electrons in the solid target material, the strong energy deposition leads to an explosive evaporation of ions, electrons and neutral atoms called the plume. The initial high pressure drives the ablation plume towards the background gas. The plume slows down and is confined in the background gas. Eventually, the atoms diffuse out of the plume and migrate to the substrate or the chamber walls [8-11]. The angular distribution of the plume atoms is influenced by the mass density of the background gas. For heavy gases the broadening of the angular distribution is bigger than the broadening in light gases. This simply means light atoms in a heavy gas are scattered much more than heavy atom in a heavy gas [12-14]. Background gas of Ar has a mass density higher than that of O_2 and therefore thus tends to reflect lighter atoms in the plume more and these results in a film with big particles on the substrate as seen in figure 5.3 (b) and figure 5.4 (b). O_2 background has a lighter mass density relative to Ar and thus results in small broadening of the angular distribution which results in a thin film with small and evenly distributed particles as seen in figure 5.3(c).

From the AFM's RMS value which is an indication of the roughness of the surface of the thin films it could be seen that films deposited in 20 mtorr Ar are more rough followed by those deposited in 20 mtorr O_2 as a background gas while films deposited in vacuum (1.6×10^{-6} mbar)

are the smoothest with an RMS value of 0.7 nm, 2.5 nm and 4.8 nm for the films deposited in vacuum, O_2 and Ar atmospheres, respectively.

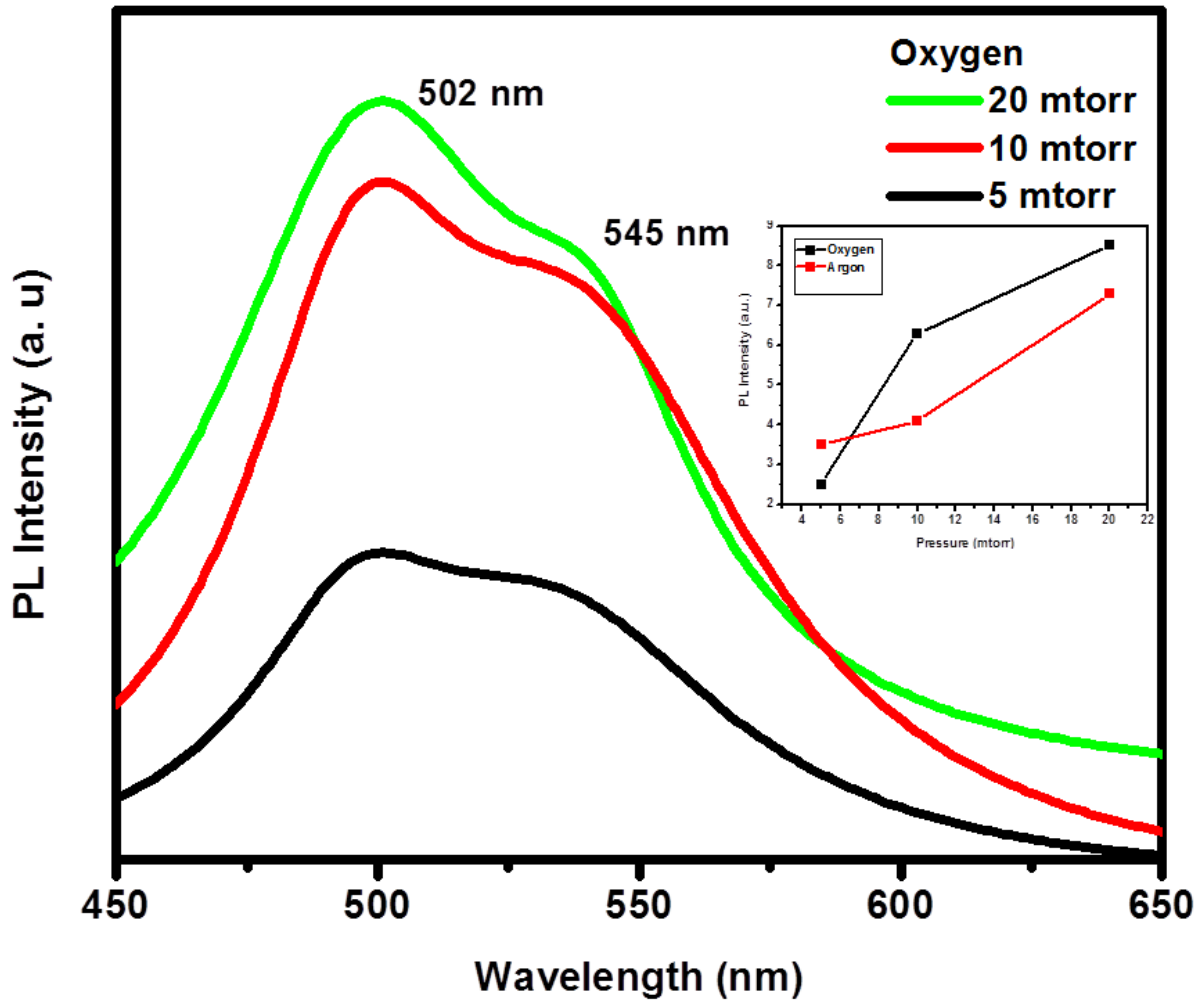

Figure 5.5: PL intensity of the films deposited in O_2 at various background gas pressures in the chamber, with the inset the relative maximum PL intensity of films deposited in O_2 and in Ar at different pressures as indicated (345 nm excitation wavelength was used).

Figure 5.5 shows the PL intensity of the films deposited in O_2 at various background gas pressures in the chamber. The emission spectra of the films were obtained under excitation of the host at 345 nm and 435 nm at room temperature. Except for the intensity difference the spectra are more or less identical with a broad peak consisting of two peaks at around 502 nm and 545 nm. These peaks are from the de-excitation of electrons from the lowest 5d level to the field split 4f ($^2f_{5/2}$ and a $^2f_{7/2}$) levels as is the case with the powder. The shape of the emission spectra of the films are identical to those of $Y_3(Al,Ga)_5O_{12}:Ce^{3+}$ in the powder form except there is a definite shift in the peak positions towards lower wavelengths. This shift can be attributed to the crystal field effect on the 5d level of the Ce^{3+} ion. The PL intensity increases with increasing pressure for both sets of films deposited in Ar and in O_2 as shown as inset in figure 5.5. This is because the increasing pressure inside the chamber slows down the particles of the plume thus preventing re-sputtering on the film surface and allows a film layer to grow. But a more intense increase is observed for films deposited in an O_2 background. This is because the O_2 molecules in the gas background will react with some of the particles of the plume and since $Y_3(Al,Ga)_5O_{12}:Ce^{3+}$ is an oxide material, the O_2 background will result in a film that has the same stoichiometry as that of the powder. PL spectra obtained by Choe [4] from annealed PLD YAG:Ce^{3+} films showed a strong and broad emission band around 570 nm and excitations at 342 and 460 nm, clearly pointed out the influence on the wavelength positions due to the Ga in our films. Figure 4.4 shows the relative placement of the 5d orbitals in $Y_3Al_5O_{12}:Ce^{3+}$ (YAG: Ce) and $Y_3(Al,Ga)_5O_{12}:Ce^{3+}$ (YAGG:Ce) [14]. Electrons are excited to the E'' state of the 5d orbital and are emitted from the E' state. The splitting of the E'' and E' states is determined by the crystal field around the Ce^{3+} ion. In films that have less Ga on the surface, the oxygen atoms around the Ce^{3+} ion are highly compressed and form a non-cubic structure. The splitting of the E'' and E'

states increases as the oxygen atoms are further distorted from the cubic structure. As more Ga atoms are deposited onto the surface of the films, oxygen atoms surrounding the Ce^{3+} ion are decompressed and form a cubic structure. As a result, the splitting between the E'' and E' states decreases with the Ga content. Consequently, the $Y_3(Al,Ga)_5O_{12}:Ce^{3+}$ films have noticeably shorter emission wavelengths (higher energy) compared to $Y_3(Al,Ga)_5O_{12}:Ce^{3+}$ powder phosphor indicating that there is more Ga in the films than in the powder. The shift in the PL wavelengths may therefore be ascribed to the slight change in environment from the powder to the thin films.

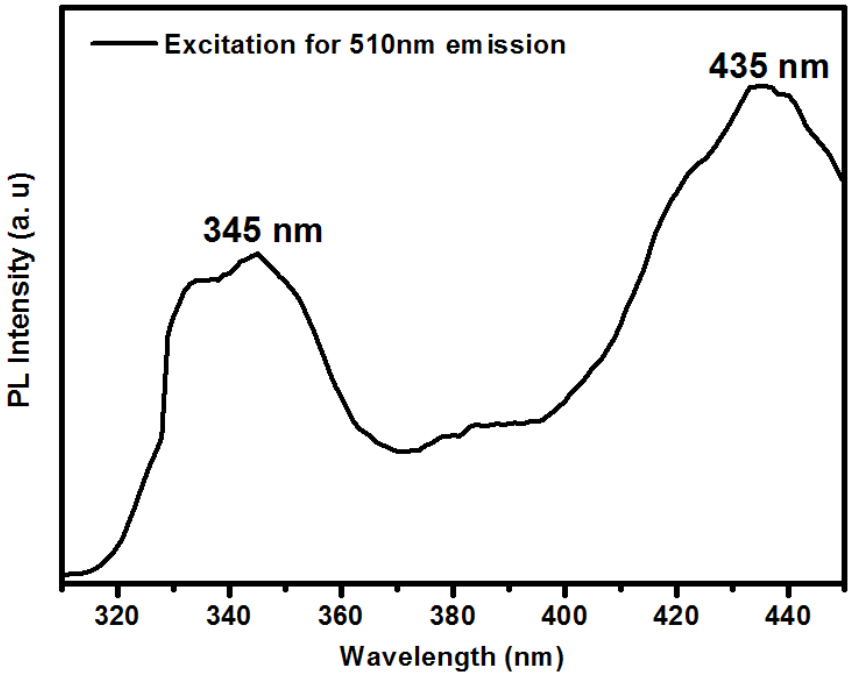

Figure 5.6: A typical excitation spectrum of the films measured for an emission of 510 nm.

The excitation spectra shown in figure 5.6 were measured from the 510 nm emission from the films. A slight shift in these peaks to lower wavelengths occurred if compared to the powder in figure 4.3. The peaks are also much broader than that of the powder with an estimated FWHM value of 33 nm and 55 nm respectively.

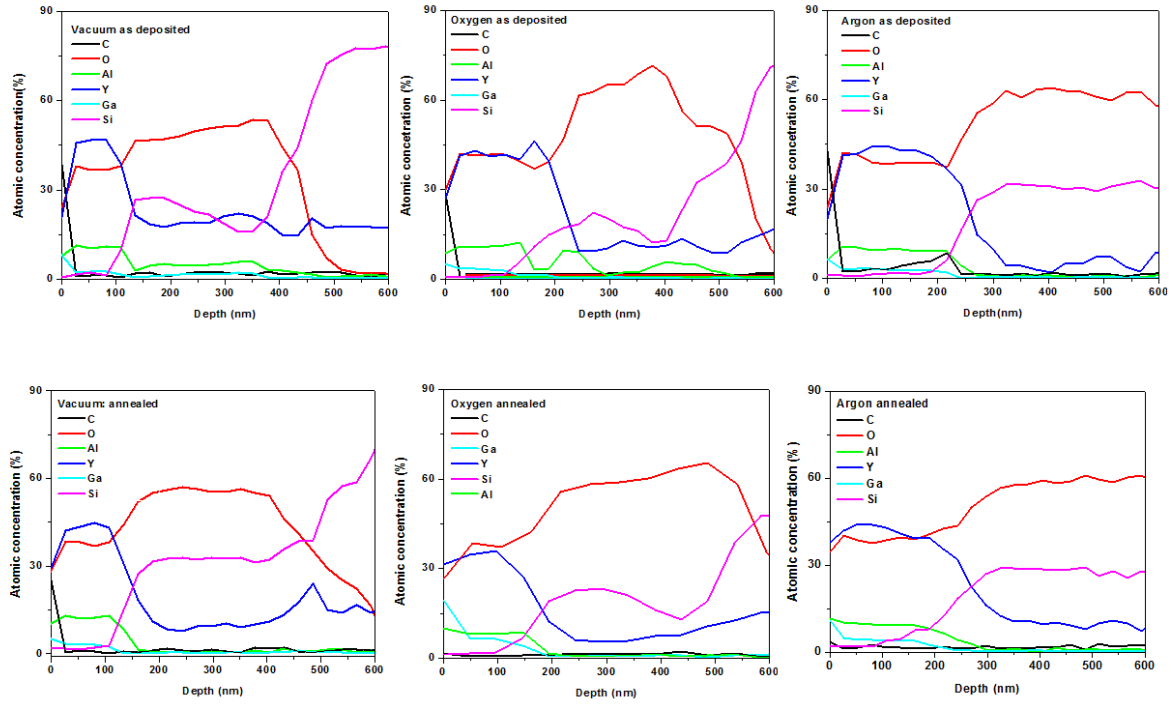

Figure 5.7: Depth profiles of films before and after annealing.

Depth profiles of several thin films as deposited and after heat treatment at 800°C in open atmosphere were performed and are shown in Figure 5.7. The depth profiles are from the $Y_3(Al,Ga)_5O_{12}:Ce^{3+}$ thin films and the SiO_2 on top of the Si substrates. By using the point (depth) where the Y concentration in the AES profiles is about 50% of the maximum Y concentration as an estimation of the film thickness the thicknesses for the vacuum, O_2 and Ar background prepared layers were determined as 120 nm, 230 nm and 270 nm, respectively. The films prepared in vacuum are clearly much thinner than the rest of the films. This might be due to the fact that the plume (in vacuum) is energetic when arriving on the substrate resulting in re-sputtering and reflection of the plume atoms which leads to the thin layer as well as a smooth surface. The effect of the Ar and O_2 atmosphere on the thicknesses is clear. It is therefore clear that the angular distribution, as pointed out above, of the plume atoms is influenced by the mass

density of the background gas and therefore the different thicknesses. The heat treatment did not change the distribution of the elements significantly except for the broader interfaces between the YAGG and the SiO_2, indicating that some diffusion did take place at the interfaces. The oxygen concentration for the O_2 background sample is slightly higher than the other films as expected causing the oxygen loss from the deposition process (light atoms in a background gas are scattered much more than heavy atom) to be filled up again to be closer to the stoichiometry of the target.

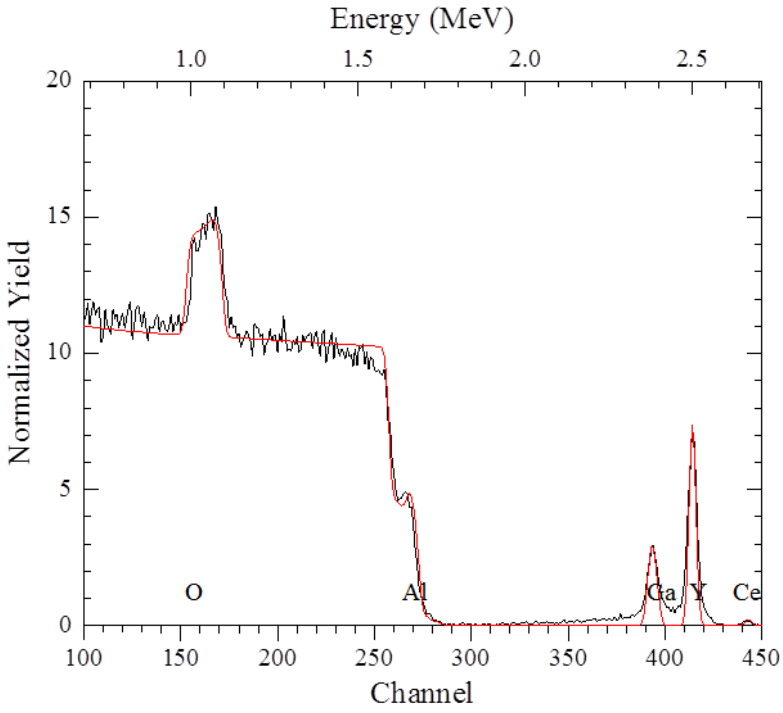

Figure 5.8: RBS spectrum of a film deposited in O_2, 20 mtorr at 300°C substrate temperature showing the best fit (red).

Figure 5.8 shows an RBS spectrum of the O_2, 20 mtorr film. The red line is the best fit simulated on the RBS data using the Rutherford universal manipulation program (RAMP) program. From the RBS the stoichiometry of the films was comparable to that of the commercial powder

(Y:Al:Ga:O – 3: 2 : 3 : 12). The RBS spectra obtained when the films were irradiated with 2Me $^4He^+$ ions looked similar for all the films.

5.4. Conclusion

Thin films of the YAGG:Ce phosphor powder were successfully prepared in different gas environments using the PLD technique. Various surface analyzing techniques were used to characterize the morphological and luminescent properties. XRD showed a slight improvement in the crystallization of the films after the films were annealed with better crystallization taking place in films deposited in an O_2 background. These films also showed the highest PL intensity when excited with a xenon lamp. The AES depth profiles indicated the films had different thickness and the distribution of elements on the layer to be homogeneous. Ablation in vacuum resulted in films with a smoother surface due to re-sputtering while ablation performed in the presence of a background gas (Ar and O_2) resulted in rougher film surfaces. PLD proved to be a good technique to grow the films of this phosphor as the RBS data showed that the stoichiometry was maintained from the powder to the film form. The results given therefore indicates that oxygen at a pressure of 20 mtorr provides good conditions in the chamber to grow films with high PL intensity and good morphological characteristics.

5.5. Acknowledgement

Special thanks to Brian Yalisi and Dr Lorinda Wu at the NLC, CSIR National Laser Centre, Rental Pool Programme, in Pretoria for assisting with the film growth using the PLD technique. Dr Coetsee-Hugo for obtaining the AES depth profiles. A special thanks to iThemba Labs in Cape Town for RBS measurements. This work is based on the research supported by the South African Research Chairs Initiative of the Department of Science and Technology and National

Research Foundation of South Africa. The University of the Free State Cluster program for financial support.

5.6. References

[1] S.W. Allison, G.T. Gillies, A.J. Rondinone, M.R. Cates, Nanotechnology. 14 (2003) 859

[2] H. Bechtel, P. Schmidt, W. Busselt, S. Baby, Schreinemacher Philips Research Europe Aachen, D-52066 Aachen, Germany; ABSTRACT A new phosphor technology for phosphor converted light-emitting

[3] H.C. Swart, E Coetzee, J.J. Terblans, O.M. Ntwaeaborwa, P.D. Nsimama, F.B. Dejene, J.J. Dolo. Physics A: Materials Science and Processing. 101(4) (2010) 633-638

[4] J. Choe, Mater. Res. Innov. 6(5-6) (2002) 238-241

[5] J.S. Bae, K.S. Shim, S.B. Kim, J.H. Jeong, S.S. Yi and J.C. Park, J. Cryst. Growth. 264 (2004) 290

[6] J. Schou, Appl. Surf. Sci. 255 (2009) 5191–5198

[8] T. Tomiki, H. Akamine, M. Gushiken, Y. Kinjoh, M. Miyazato, T. Miyazato, N. Toyokawa, M. Hiraoka, N. Hirata, Y. Ganaha, and T. Futemma, J. Phys. Soc. Jpn. 60(7) (1991) 2437–2445

[9] http://www.phosphoo-technology.com/products/ctr.htm [Accessed 29 May 2012]

[10] S. Amoruso, R. Bruzzese, N. Spinelli, R. Velotta, M. Vitiello, X. Wang, Phys. Rev. B 67 (2003) 224503

[11] S. Amoruso, B. Toftmann, J.Schou, Phys. Rev. E. 69 (2004) 056403

[12] H.C. Lee, D.E. Zeitoun, J.D. Parisse, M. Sentis, W. Marine, Phys. Rev. E. 62 **(**2000) 4152

[13] Y. Nakata, W.K.A. Kumuduni, T. Okada, M. Maeda, Appl. Phys. Lett. 64 (1994) 2599

[14] J.M. Warrander, M.J. Aziz, Phys.Rev.B. 75(2007) 085433

Chapter 6

The effect of substrate temperature on the structure, morphology and photoluminescence properties of pulsed laser deposited $Y_3(Al, Ga)_5O_{12}:Ce^{3+}$ nano thin films.

6.1. Introduction

$Y_3Al_5O_{12}:Ce^{3+}$ or YAG:Ce is used in several applications such as solid state lighting and displays. When Ga is added and substituted for Al to form $Y_3 (Al,Ga)_5O_{12}:Ce^{3+}$, this phosphor has the potential to be applied in the fabrication of Light emitting diodes especially if the phosphor is used in the thin film form. Thin films offers several advantages due to their good luminescence characteristics, higher image resolution from small grains, better thermal stability and good adhesion to the substrate [1]. The substrate temperature plays a critical role in the growth of the films during the Pulsed Laser Deposition (PLD). The mobility of the atoms deposited on the surface is directly dependent on the temperature of the substrate. The activation energy of processes that takes place on the surface is influenced by this dependency [2]. The movement and interaction on the surface of the substrate of different particles (atoms, ions, electrons etc.) that makes up the plume is mainly determined by the substrate temperature and the energy of these deposited particles [3]. The crystallinity of the as-grown films has been shown to be highly dependent on the processing temperature [4]. Research on the influence of substrate temperature on $Y_3(Al,Ga)_5O_{12}:Ce^{3+}$ thin films is of great importance to establish the

optimum substrate temperature range for a high photoluminescence (PL) intensity. In this chapter we report on the luminescence and morphological properties of $Y_3(Al,Ga)_5O_{12}:Ce^{3+}$ thin films prepared by PLD. The aim was to establish the optimum substrate temperature that will produce thin films with a high PL intensity as well as structural properties similar to the $Y_3(Al,Ga)_5O_{12}:Ce^{3+}$ phosphor in the powder form.

6.2. Experimental Setup

$Y_3(Al,Ga)_5O_{12}:Ce^{3+}$ powder phosphor obtained from Phosphor Technology (UK) with Commission Internationale de l'Eclairage (CIE) coordinates: (x=0.306, y=0.521) and non-uniform particles with median particle size of 2.5 μm were used in this study [5]. The Ga to Al ratio is about 60:40 in the $Y_3(A,Ga)_5O_{12}:Ce^{3+}$ crystal structure. The powder was pressed without binders to make a pellet which was used as a target for PLD. Si (100) wafers were used as substrates. They were cut into approximately 2 cm by 2 cm pieces and cleaned in an acetone ultrasonic bath for 15 minutes. A layer of SiO_2 was grown on some of the Si substrates. The phosphor target and one Si piece at a time were inserted into the PLD chamber. An Nd:YAG 266 nm laser was used for the deposition. The laser fluency was kept at 0.78 J/cm^2 with a 10 Hz frequency. The target to substrate distance was kept at 6 cm. The chamber was evacuated to a base pressure of 3.7×10^{-6} torr. Then the chamber was backfilled with O_2 gas to a chamber pressure of 1×10^{-2} torr. The ablation was performed for substrate temperatures of 22°C, 100°C, 300°C and 500°C. The room temperature samples were deposited on the Si(100) without SiO_2, while the higher temperature samples were deposited on the Si/SiO_2 substrates. The films were then annealed at 800°C for 2 hours in open air. Atomic Force Microscopy (AFM) was used to obtain micrographs of the surface using the Shimadzu SPM – 9600 model. PL excitation and emission spectra ware recorded using a Cary Eclipse fluorescence spectrophotometer (Model: LS

55) at room temperature using a 140 W monochromatized Xenon flash lamp as an excitation source. X-Ray Diffraction (XRD) data was collected by using a D5000 diffractometer using CuKα radiation of λ = 1.5405 nm in the 2θ range from 24° – 40°, with a counting time of 2 s for each step size of 0.0302°. Auger Electron Spectroscopy (AES)'s depth profiles and AES survey test of the surface where performed using a PHI 700 Scanning Auger Nanoprobe. AES surveys were done with a 25 kV 10 nA electron beam. Depth profiles were done by sputtering with a 2 kV, 2 μA ion beam, at 1x1 mm raster area with a sputter rate of 27 nm per min. Scanning Electron Microscope (SEM) images were obtained with a 25 kV, 10 nA electron beam. Line profiles were done with a 25 kV, 10 nA electron beam.

6.3. Results

Figure 6.1 shows the XRD patterns of the films ablated at different substrate temperatures together with the powder pattern. The ICSD file number 29250 is also shown. Crystalline thin films with the same cubic polycrystalline phase structure as the powder were obtained during the PLD. XRD results show a constraint in the growth of the crystals due to a low atomic mobility at a deposition temperature of 22°C. An increase to 100°C and 300°C supplied the atoms on the substrate surface with more thermal energy and thus increased their surface mobility that lead to better crystallization at the higher temperatures. However too high temperatures such as 500°C can decrease the crystallinity of the thin films due to interdiffusion, desorption or dissociation of atoms and molecules.

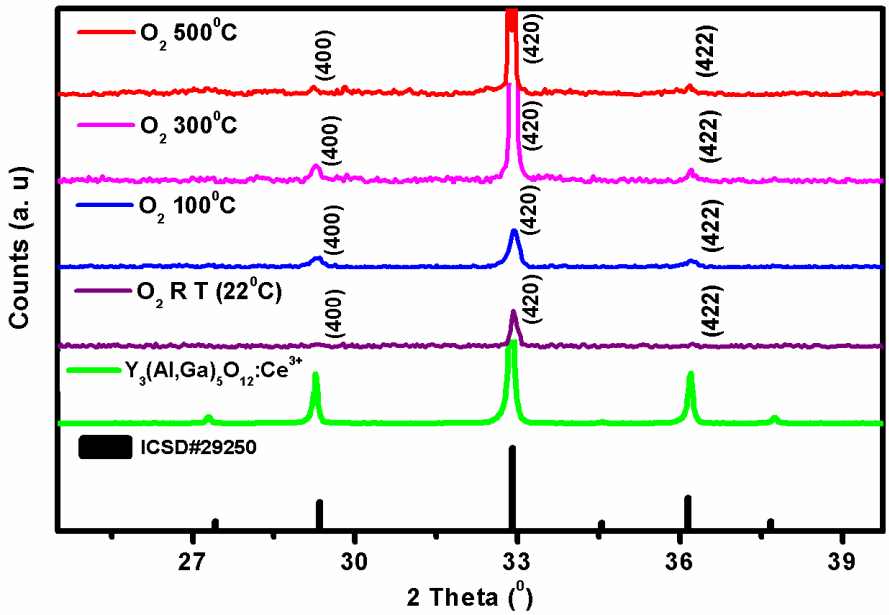

Figure 6.1. XRD patterns of $Y_3(A,Ga)_5O_{12}:Ce^{3+}$ powder and films deposited at different substrate temperatures.

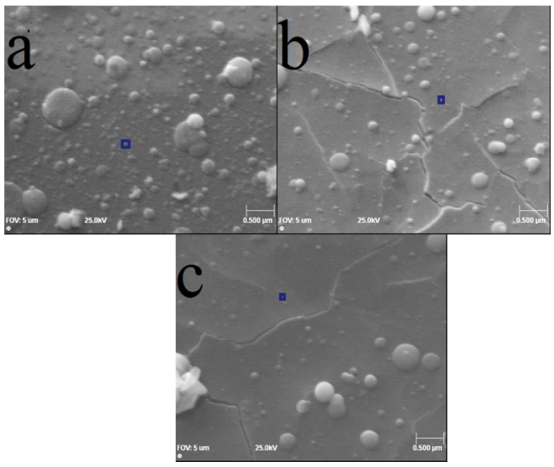

Figure 6.2. SEM images of films ablated at substrate temperatures of (a) 22°C, (b) 300°C and (c) 500°C.

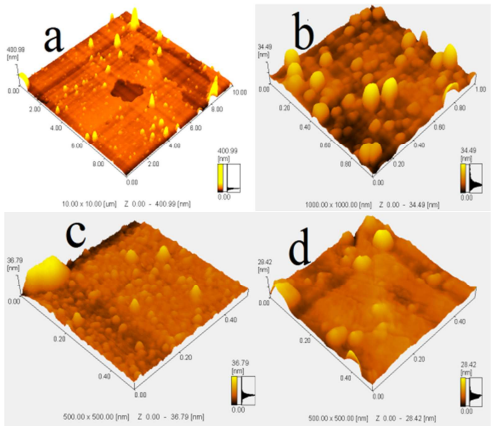

Figure 6.3. AFM images of films ablated at substrate temperatures of (a) 22°C, (b) 100°C (c) 300°C and (d) 500°C.

Effects of substrate temperature on the morphological properties of $Y_3(Al,Ga)_5O_{12}:Ce^{3+}$ thin films are shown in figure 6.2 and figure 6.3. For a substrate temperature of 300°C, a well-defined

grain growth is obtained seen on the AFM image in figure 6.3(c). A lack of uniformity is observed for films ablated at 22°C (figure 6.2(a) and figure 6.3(a)) where big and small particles are seen due to the low mobility of the atoms on the surface of the substrate. Figure 6.3(b) shows a better grain growth but with big and small particles still seen. A poor defined grain growth resulted for films ablated for a substrate temperature of 500°C. For these films shown in figure 6.2 (c) and 6.3 (d), the surface appears melted with a decreased in surface roughness due to the high substrate temperature.

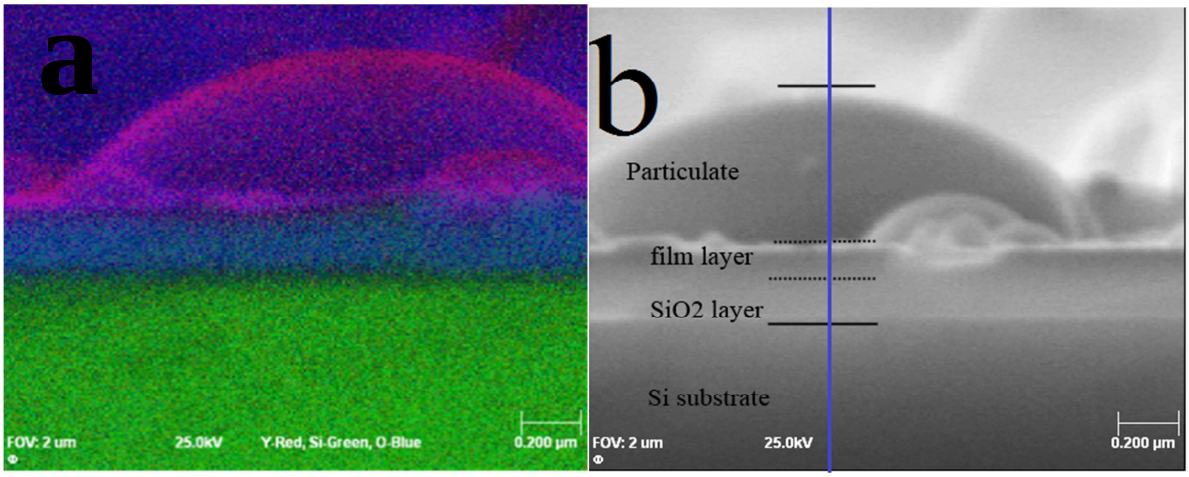

Figure 6.4. (a) Cross sectional SAM image and (b) cross sectional SEM image of the film ablated at a substrate temperature of 300°C.

Figure 6.4 (a) and (b) show a typical cross sectional SAM image and (b) cross sectional SEM image of the film ablated at a substrate temperature of 300°C. Different regions and layers are indicated by solid and dotted lines on the cross sectional SEM image. It is clear that the deposited film consist of a homogenous thin film and additional big particulates of several hundred nanometer on top of the film. The uniform phosphor layer thickness was estimated at about 160 nm. Similar images were obtained for the other films. The generation of particulates

during the deposition process, is not ideal for the application field and is one of PLD's disadvantages. However Coetsee et al. [6] pointed out that these particulates may have an advantage due to the higher CL intensity coming from these particles on the thin film. During the investigation of the CL intensity degradation of tin oxide coated Y_2SiO_5:Ce thin films grown by PLD it was observed that more photons exiting these spherically shaped particles in comparison with the uniform thin layer where the photon get totally internally reflected [6]. The depth profiles were performed at the positions on the surface (indicated by the blue squares in the SEM images in figure 6.2) between these big particles and are shown in figure 6.5.

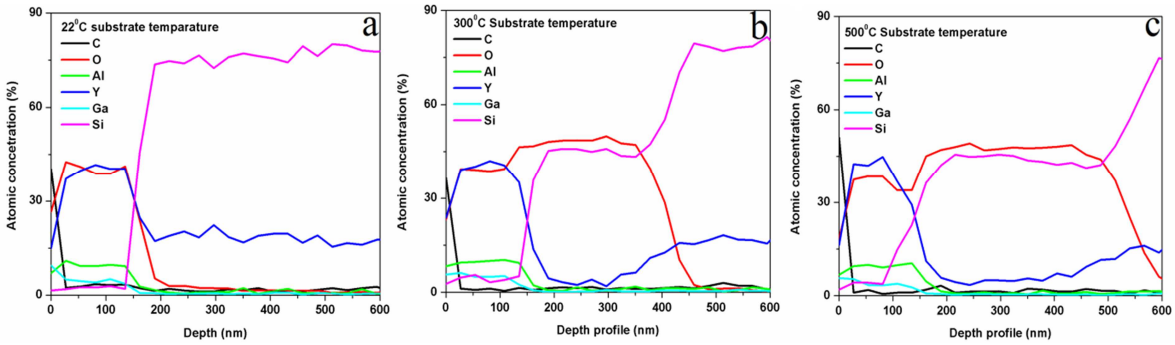

Figure 6.5. Depth profiles of the different substrate temperature films.

Figure 6.5 shows depth profiles of the films deposited at (a) 22°C, (b) 300°C and (c) 500°C. The depth profiles are from the $Y_3(Al,Ga)_5O_{12}:Ce^{3+}$ thin films and the SiO_2 on top of the substrates. A much higher Y concentration as expected was obtained at all the substrate temperatures. By using the point (depth) where the Y concentration is about 50% of the maximum Y concentration as an estimation of the film thicknesses for the 22°C, 300°C and 500°C prepared layers, the thicknesses were determined as 152 nm, 153 nm and 144 nm respectively. Similar thickness values were also found for cross sectional measurements of the films. All the films seem to have almost the same thickness and substrate temperature does not have a significant effect on this

regard. The concentration of the elements making up the films also remain more or less the same as the substrate temperature is varied. Please note that Y is not actually diffusing into the SiO_2 layer as observed on the depth profiles. What is seen as Y concentration increasing inside the SiO_2 layer is actually as a result of the Si 1739 eV peak from SiO_2 monitored overlapping with the Y 1748 eV peak and need to be removed in future studies. The distribution of elements, however, is significantly affected at the interface of the phosphor/SiO_2 at the higher substrate temperature during deposition as indicated by the depth profile of the film deposited at the 500°C substrate temperature (figure 6.5 (c)). It can be seen that the Si has diffused into the phosphor thin film with the consequent broadening of the interface. The 500°C substrate temperature seems to promote this diffusion of Si into the phosphor thin film layer.

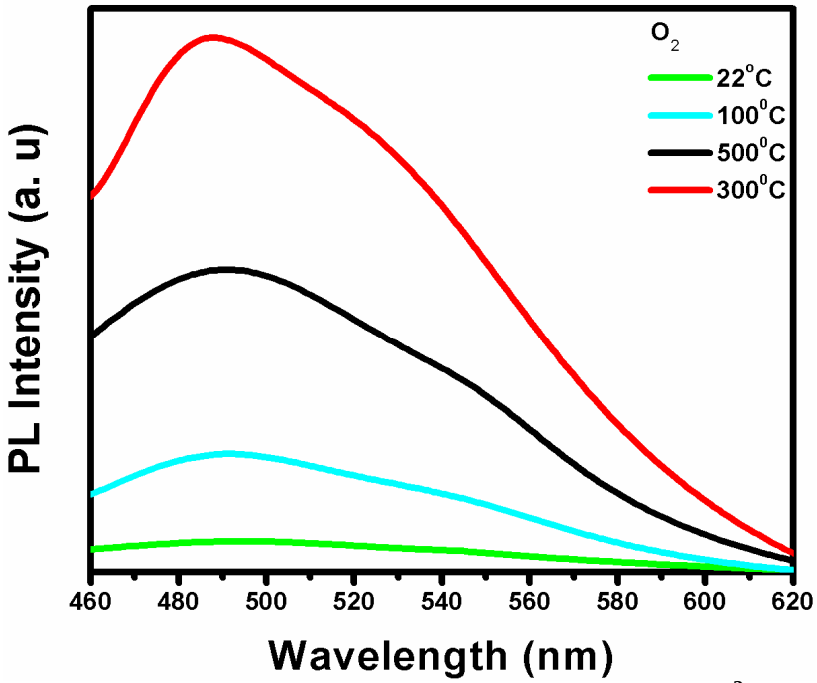

Figure 6.6. PL intensity of the films deposited in 1×10^{-2} torr O_2 at various substrate temperatures (Extation wavelength = 345 nm).

$Y_3(Al,Ga)_5O_{12}:Ce^{3+}$ in powder form has 60% Ga and 40% Al, this results in the PL emission wavelength of 512 nm and 565 nm [7]. Figure 6.6 shows the PL emission of $Y_3(Al,Ga)_5O_{12}:Ce^{3+}$ thin films which peaks at around 495 nm and 542 nm. This wavelength shift can be attributed to the change in Ga/Al ratio within the crystal lattice which primarily affects the crystal field around the Ce ion which is responsible for the emission. Ce^{3+} doped phosphors typically have two emission bands due to the true levels of $^2F_{5/2}$ and $^2F_{7/2}$ of the configuration of Ce^{3+} [8, 9]. Each Ce^{3+} site gives rise to transitions from the 5d to the two (therefore two peaks) 4f energy levels ($^2F_{5/2}$ and $^2F_{7/2}$ due to crystal field splitting). The substitution of Ga into the $Y_3Al_5O_{12}:Ce^{3+}$ lattice result in a decompression of oxygen atoms directly coordinated to the Ce^{3+} ion and the structure becomes more cubic. This change in structure directly affects the 5d orbitals of the Ce^{3+} as it moves it from the bottom of the conduction band and likewise the PL characteristics as seen by the shift in figure 6.6 [10]. It can also be seen from figure 6.6 that the PL intensity increased with an increasing substrate temperature up to 300 °C. Substrate temperature improved the crystallinity and luminescent intensities of thin film phosphors. Interdiffusion of the Si at 500°C however lead to a decrease in the PL intensity. Cho *et al*. [11] noted the same effect during the investigation of optical properties of sol-gel derived $Y_2O_3:Eu^{3+}$ thin film phosphors for display applications.

6.4. Conclusion

Thin films of the $Y_3(Al,Ga)_5O_{12}:Ce^{3+}$ phosphor powder were successfully prepared at different substrate temperatures using the PLD technique. XRD showed that the crystallinity of the films has improved with increasing substrate temperature up to 300°C. The crystallinity was affected by interdiffusion at 500°C. The films deposited at 300°C also showed the highest PL intensity. AFM images showed nano-meter sized grains in the range of 30 nm to 90 nm and at a 22°C

substrate temperature there was a mixture of small and large grains. As the substrate temperature was increased to 300°C larger and more uniform grains formed that increased the surface roughness. At 500°C, a decrease in the surface roughness was, however, observed. The results indicate that a substrate temperature of 300°C in an O_2 atmosphere provides good conditions to grow films with high PL intensity and good morphological characteristics.

6.5. Acknowledgments

Gratitude to Brian Yalisi and Dr Lorinda Wu at the NLC, CSIR in Pretoria for assisting with the film growth using the PLD technique. Dr Coetsee-Hugo for NanoSAM measurements. This work is based on the research supported by the South African Research Chairs Initiative of the Department of Science and Technology and the National Research Foundation of South Africa. The University of the Free State is acknowledged for financial support.

6.5. References

[1] J.S. Bae, K.S. Shim, S.B. Kim, J.H. Jeong, S.S Yi, J.C. Park, J. Cryst. Growth. 264 (2004) 290

[2] S. Christoulakis, M. Suchea, N. Katsarakis, E. Koudoumas, Appl. Surf. Sci. 253 (2007) 8169

[3] X.M. Fan, J.S. Lian, Z.X Guo, H.J. Lu, Appl. Surf. Sci. 239 (2005) 176

[4] R. Eason (Editor), Pulsed laser deposition of thin films application-led growth of functional materials, Wiley Interscience, 2006

[5] http://www.phosphoo-technology.com/products/ctr.htm [Accessed 29 May 2012]

[6] E. Coetsee, H.C. Swart, J. J Terblans, J. Vac. Sci. Technol. A 25 (2007) 4

[7] S.T.S. Dlamini, H.C. Swart, O.M. Ntwaeaborwa, 2013 Sol. State Sci. 23 (2013) 65-71

[8] R. Hua, B. Lei, D. Xie, C. Shi, J. Solid State Chem. 175 (2003) 284

[9] T.A. Obrien, P.D. Rack, P.H. Holloway, M.C. Zerner, J.Lumin. 78 (1998) 245

[10] J.L. Wu, G. Gundiah, A. K. Cheetham, Chem. Phys. Lett. 441 (2007) 250

[11] J.Y. Cho, K. Ko, Y.R. Do, Thin Solid Films. 515 (2007) 3373

Chapter 7

Characterization of $Y_3(Al, Ga)_5O_{12}:Ce^{3+}$ thin films.

This chapter contains extra and supporting discussions on the characterization of thin films in order to investigate surface morphology with different PLD process parameters when preparing thin films. The results given in this chapter from SEM and AES measurements adds to what have been discussed in Chapter 5 and Chapter 6. The influence of the number of pulses on photoluminescence properties of the thin film is also briefly discussed.

7.1. Introduction

In pulsed laser deposition (PLD) technique, different parameters such as background gas in the deposition chamber, substrate temperature and the number of laser pulses have a direct influence on morphological properties of $Y_3(Al,Ga)_5O_{12}:Ce^{3+}$thin film. Particle formation is a major drawback of PLD and it usually is the main limiting factor in the application field of this deposition method. Particulates can form from liquid droplets that are expelled from the target during ablation, from ejected protruding surface features that are mechanically removed from the target by laser induced thermal and mechanical shock, or from cluster condensation from vapour species due to supersaturation[1]. A number of particulate control measures have been devised over the years to reduce particulate formation on the film surface during PLD. Some of these control measures include second laser for vaporization of particulates in plume [2,3,4] and

Ambient gas control [1]. Thin films of $Y_3(Al,Ga)_5O_{12}:Ce^{3+}$ were prepared using PLD and the morphological properties of the films were investigated. Different deposition parameters such as background gas, substrate temperature and number of laser pulses were varied.

7.2. Experimental

$Y_3(Al,Ga)_5O_{12}:Ce^{3+}$ powder phosphor obtained from Phosphor Technology (UK) with Commission Internationale de l'Eclairage (CIE) coordinates: (x=0.306, y=0.521) and non-uniform particles with median particle size of 2.5 μm were used [5]. The Ga to Al ratio was about 60:40 in the $Y_3(Al,Ga)_5O_{12}:Ce^{3+}$ crystal structure. The powder was first pressed without binders to make a pellet which was used as a target for ablation. Oxidized silicon (100) wafers (SiO_2/Si) were used as substrates. They were first cut into approximately 2 cm by 2 cm pieces and cleaned in an acetone ultrasonic bath for 15 minutes. The target was ablated using a 266 nm Nd:YAG laser and the resulting plume was deposited on SiO_2/Si substrates (one at a time) placed perpendicular to the target at a fixed target-substrate distance of 6 cm . The laser fluence and frequency were kept constant at 0.78 J/cm^2 and 10 Hz respectively. The depositions of the $Y_3(Al,Ga)_5O_{12}:Ce^{3+}$ films were carried out when varying parameters such as substrate temperature (from room temperature up to 500°C), the number of pulses (10 000 to 40 000) and the chamber atmospheres (O_2, Ar and vacuum). The deposition chamber was first evacuated to a base pressure of 1 x 10^{-6} mbar. To investigate the effect of the number of pulses from the laser on the growth of the $Y_3(Al,Ga)_5O_{12}:Ce^{3+}$ films, the chamber was backfilled with O_2 gas at 10 mtorr pressure and ablation was done while the number of pulses from the Nd:YAG laser was varied from 10 000, 20 000 and 40 000 pulses with the substrate temperature kept constant at 300°C. Then to investigate the effect of substrate temperature, the number of pulses were kept constant at 20 000 pulses and the ablation was done at the substrate temperatures of 22°C (Room

Temperature), 300°C and 500°C for chamber atmospheres of 10 mtorr O_2. For the investigation of the effects of PLD chamber atmospheres, the substrate temperature and the number of pulses were kept constant at 300°C and 20 000 pulses respectively. Ablation was first done in the chamber with a vacuum pressure of 10^{-6} mbar, then in O_2 and Ar atmospheres at pressure of 20 mtorr, respectively for both gases. A summary of deposition parameters that show parameters that were varied versus those that were fixed is given in Table 7.1.

Table 7.1: Varied vs. fixed parameters during film deposition

Fixed Parameters		**Varied Parameters**			
Laser fluence (J/cm^2)	0.76	Substrate temperature (°C)	22	300	500
Target distance (cm)	6	No of Pulse	10 000	20 000	40 000
Frequency (Hz)	10	Working atmosphere	Ar (mtorr)	O_2 (mtorr)	Vacuum (mtorr)
		Working pressure	20	20	10^{-6}

The films were later annealed in air at 800°C for 2 hours to improve their crystallinity and optical properties. The root mean square (RMS) values were calculated using the commercial software of the AFM system. The room temperature PL excitation and emission spectra were recorded using a Cary Eclipse fluorescence spectrophotometer (Model: LS 55) using a 140 W monochromatized Xenon flash lamp as an excitation source. Auger depth profile survey surface testing was performed using a PHI 700 Scanning Auger Nanoprobe. The surveys were done with a 25 kV, 10 nA electron beam. For depth profiling, the film surfaces were sputtered with a 2 kV, 2 µA ion beam, over a 1x1 mm raster area with a sputter rate of 27 nm per min. SEM images were done with 25kV, 10 nA electron beam

7.3. Results

Figure 7.1 shows emission spectra of films deposited with different number of pulses in an O_2 atmosphere at a pressure of 10 mtorr with substrate temperature kept constant at 300°C. The frequency of the laser was 10 Hz. The deposition was done at 10 000, 20 000 and 40 000 pulses which is equivalent to ablation times of 16 min 40 s, 33 min 20 s and 66 min 40 s respectively. The PL intensity of the films increases with increasing number of pulses as expected due to a thicker layer that was deposited at a larger number of pulses.

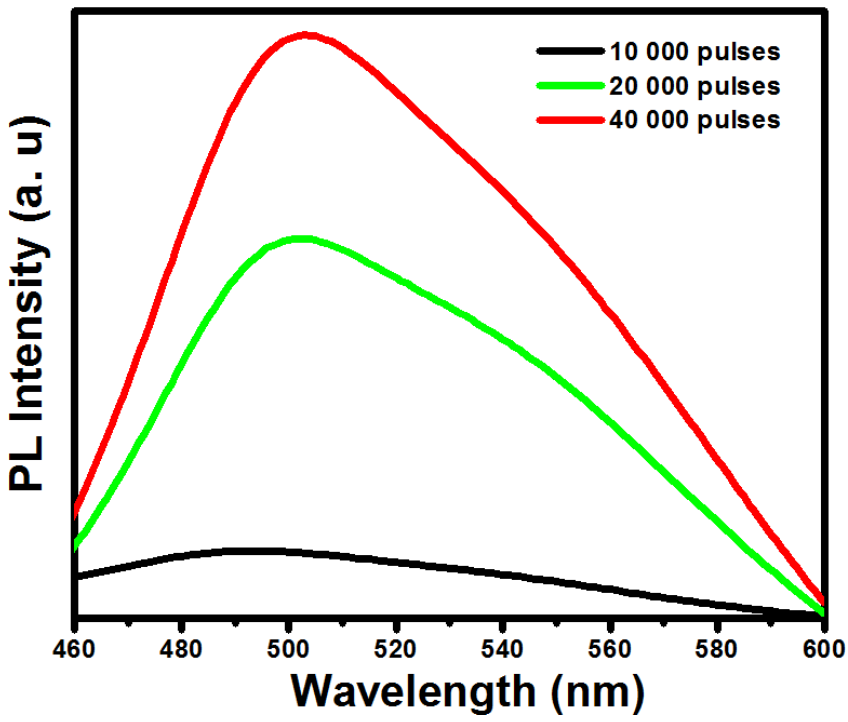

Figure 7.1: Emission spectra of films deposited with different number of pulses in an O_2 atmosphere at a pressure of 10 mtorr with substrate temperature kept constant at 300°C.

Longer period of deposition or high number of pulses results in more material being ablated from the target and deposited onto the substrate. This result in thicker films which means high content

of all the elements making up the $Y_3(Al,Ga)_5O_{12}:Ce^{3+}$ phosphor are present on the surface. Ce^{3+} ions are also ejected from the target and incorporated into the garnet lattice on the films and this is fundamental in order to obtain high PL emission from films of micro/nano thickness. Except for the difference in the PL intensity all the spectra are more or less identical with a broad peak consisting of two peaks around 500 nm and 545 nm (not clearly visible). These peaks are from the de-excitation of electrons from the lowest 5d level to the crystal field split 4f ($^2F_{5/2}$ and a $^2F_{7/2}$) levels as it was observed from the same material in powder form [6]. The shape of the emission spectra of the films are identical to those of $Y_3(Al,Ga)_5O_{12}:Ce^{3+}$ in the powder form except that there is a definite shift in the peak positions towards lower wavelengths. This shift can be attributed to the crystal field effect on the 5d level of the Ce^{3+} ion [7].

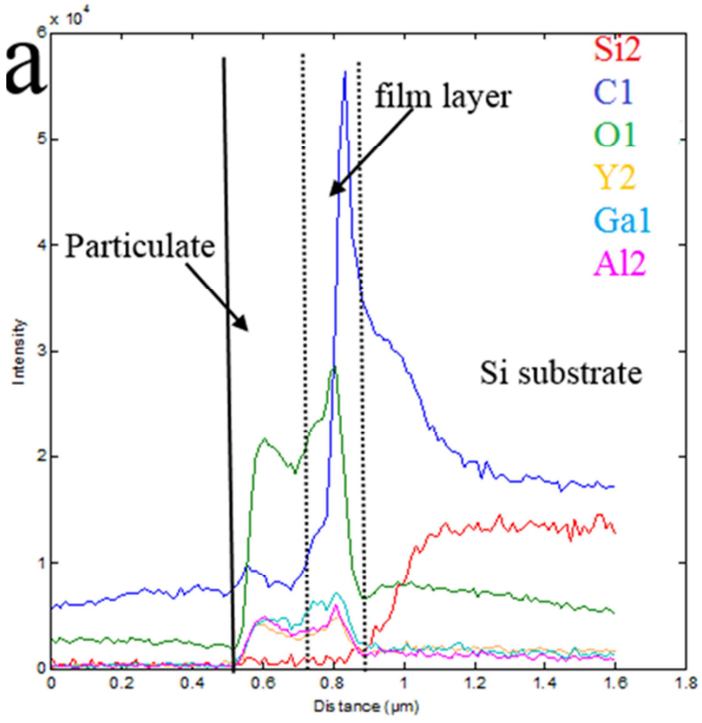
a
x 10^4
Si2
C1
O1
Y2
Ga1
Al2
film layer
Particulate
Si substrate
Intensity
Distance (μm)

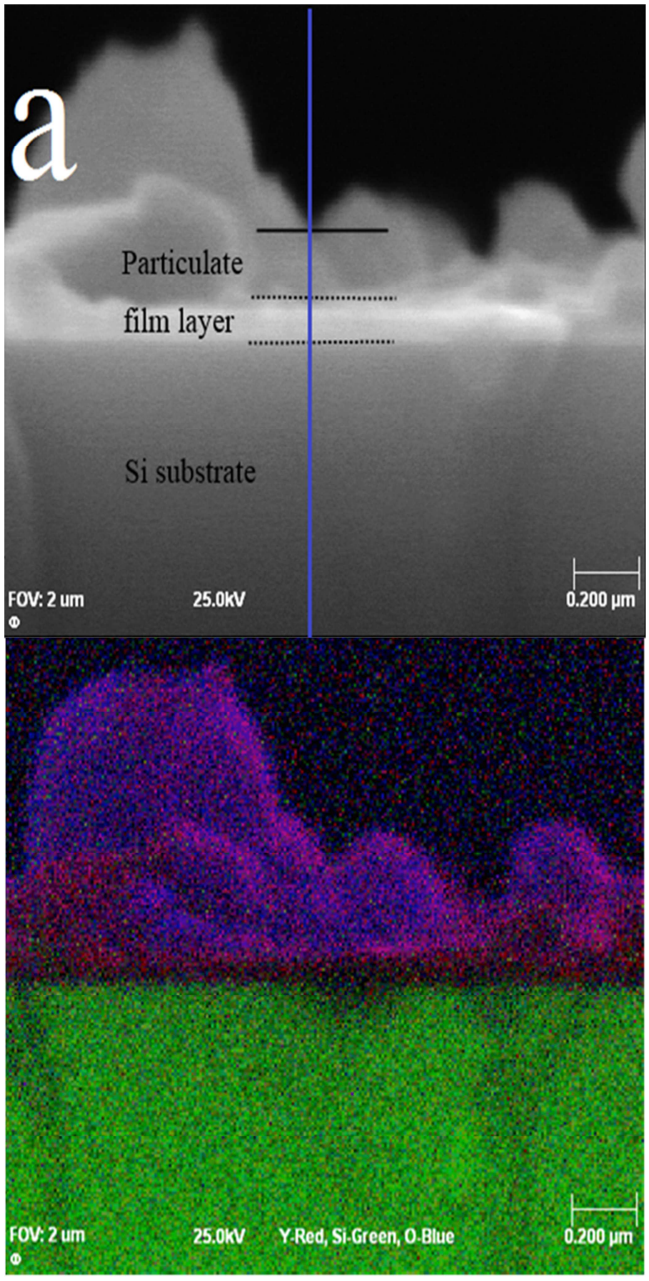
a
Particulate
film layer
Si substrate
FOV: 2 um
25.0kV
0.200 μm
FOV: 2 um
25.0kV
Y-Red, Si-Green, O-Blue
0.200 μm

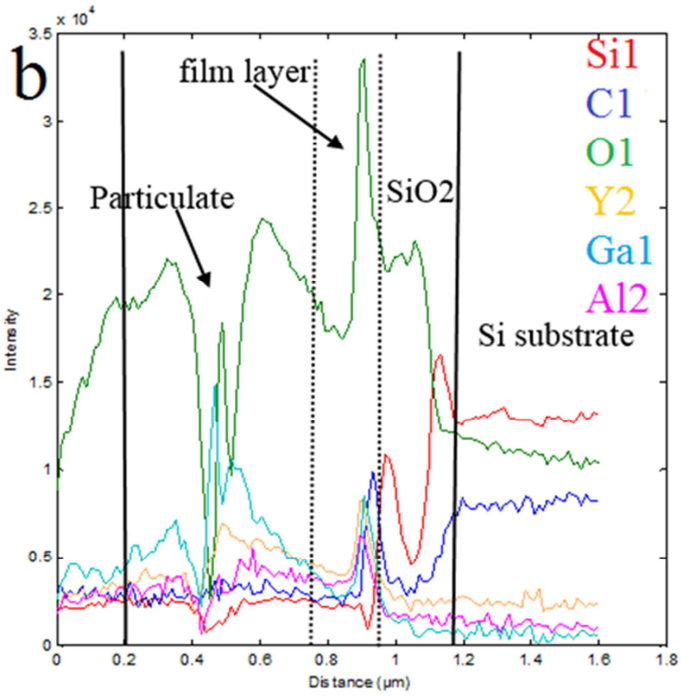
b
x 10^4
film layer
Particulate
SiO2
Si substrate
Si1
C1
O1
Y2
Ga1
Al2
Intensity
Distance (μm)

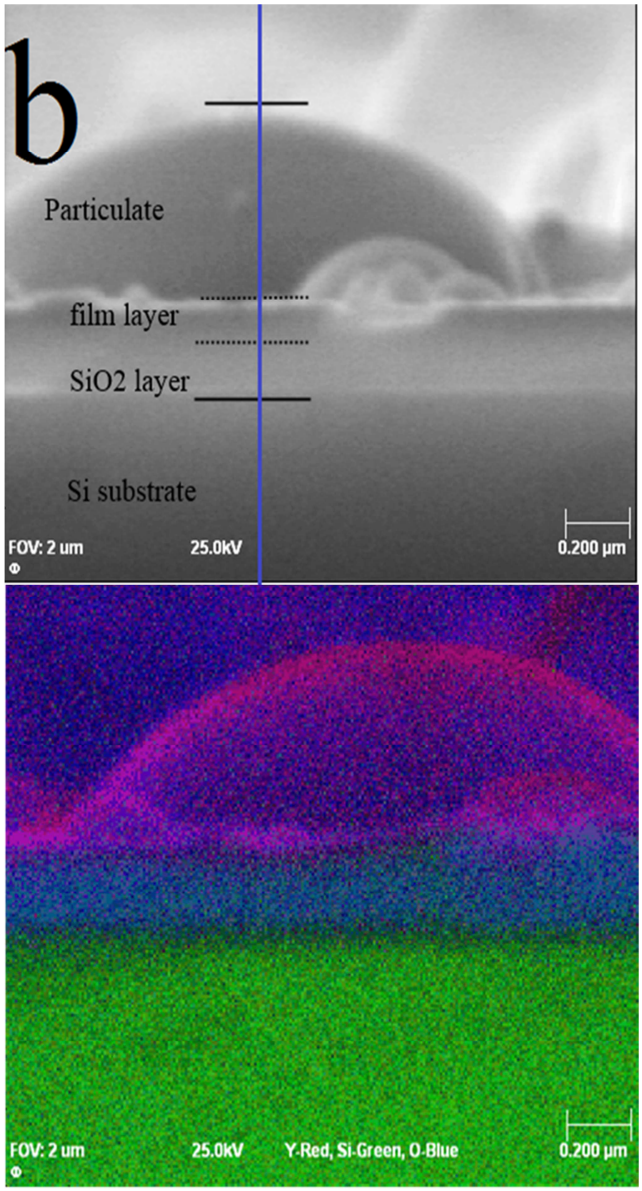
b
Particulate
film layer
SiO2 layer
Si substrate
FOV: 2 um
25.0kV
0.200 μm
FOV: 2 um
25.0kV
Y-Red, Si-Green, O-Blue
0.200 μm

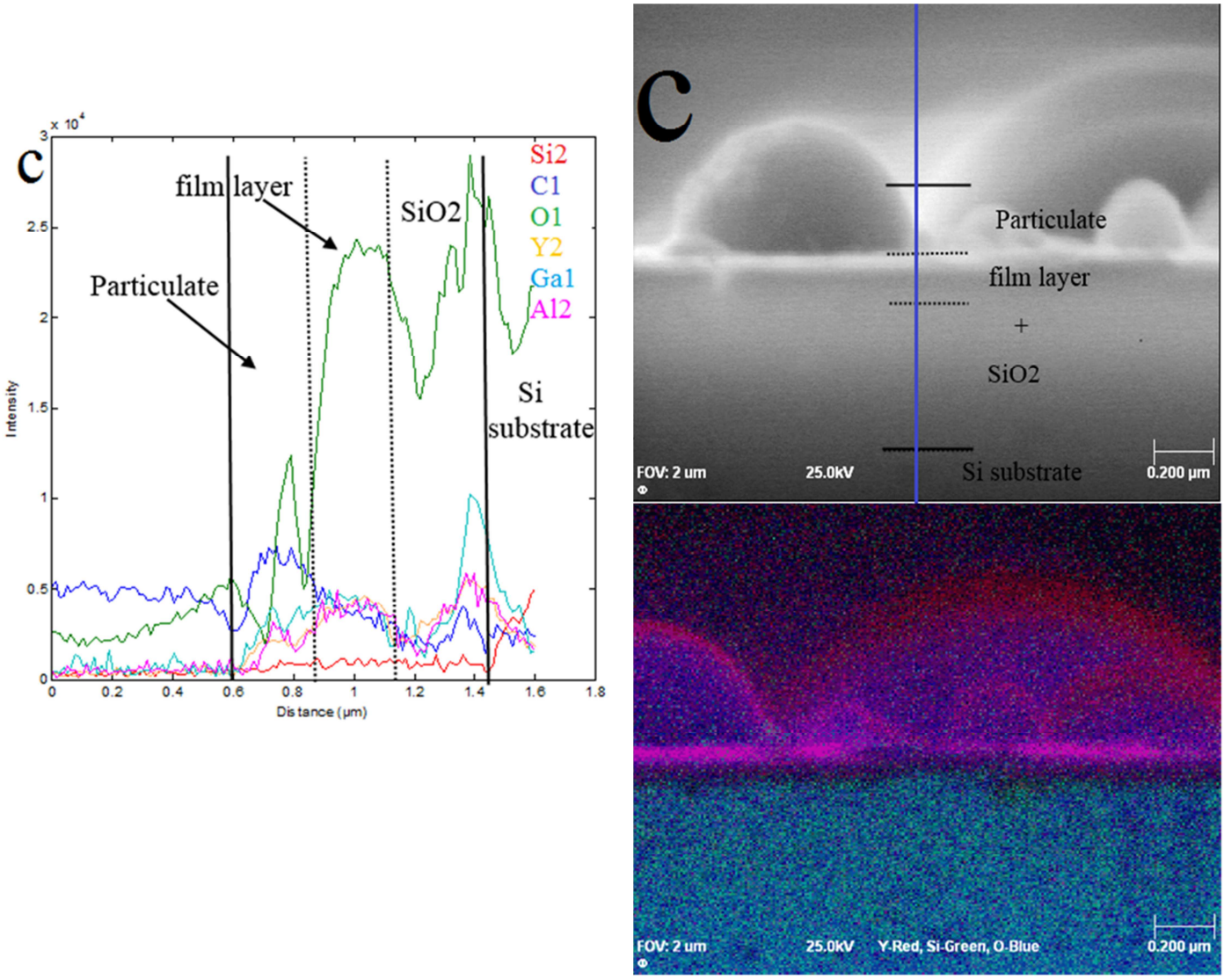

Figure 7.2: The cross sectional SEM images together with the cross sectional SAM image and AES survey of the films ablated at substrate temperatures of (a) 22˚C, (b) 300˚C and (c) 500˚C

The effects of substrate temperature have already been discussed in chapter 6 where the analysis indicated the substrate temperature of 300˚C in an O_2 atmosphere provided good conditions for film growth with high PL intensity. From Figure 7.2, the thickness of the films can be measured directly from the images. The thickness obtained when measured from the cross sectional images

is equivalent to the thickness obtained from the AES depth profiles reported in chapter 6, section 6.3. The thickness ranges from 135 nm to 155 nm when measure from the images where 0.2 μm ≈ 9mm. Also from Figure 7.2, it can be seen from the cross sectional SEM images that formation of particulates on the surface still persist at different substrate temperatures. Therefore substrate temperature could not be optimized for prevention of particulates on the film surface.

The background atmosphere of the chamber however does seem to play a role in the reduction of particulate formation on the surface of the films. AFM's RMS value which is an indication of the roughness of the surface of the thin films is shown in figure 7.3 and it can be seen that films ablated in Ar are the roughest followed by those ablated in O_2 as a background gas while films ablated in vacuum are the smoothest with RMS value of 0.7 nm for the film ablated in vacuum and RMS values of 2.5 nm and 4.8 nm for the ones ablated in Ar and O_2 background respectively.

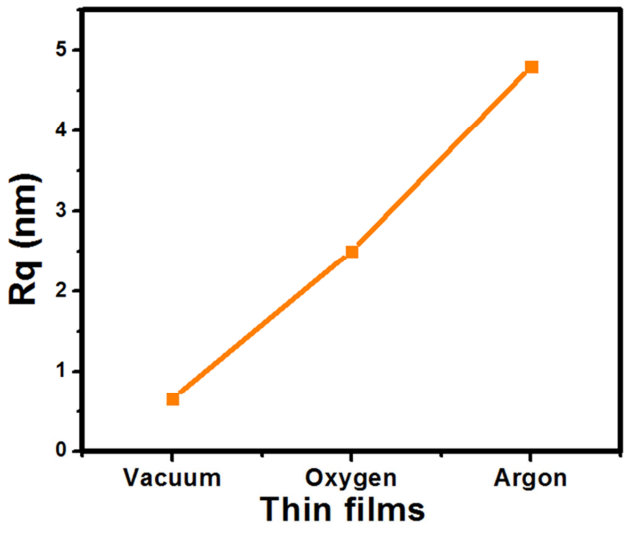

Figure 7.3: AFM's RMS value of different films at various background atmospheres.

SEM images of the films ablated in various background atmospheres are shown in Figure 7.4 and they show more particulate growth in films ablated in Ar atmosphere as compared to those ablated in O_2 and in vacuum. Figure 7.4(a) shows a relatively small number of particulates on the surface as compared to Figure 7.4(b) and (c) does supporting the AFM's RMS results shown in Figure 7.3. Typical particulate sizes are in the micron and submicron ranges. SEM images show a small size distribution in Figure 7.4(a) but an increase in the particle size with pressure is observed in Figure7.3(b) and (c). Similar result of more particulate forming and increase their size due to the presence of the background gas or increase in the chamber atmosphere are reported elsewhere [1] [8]

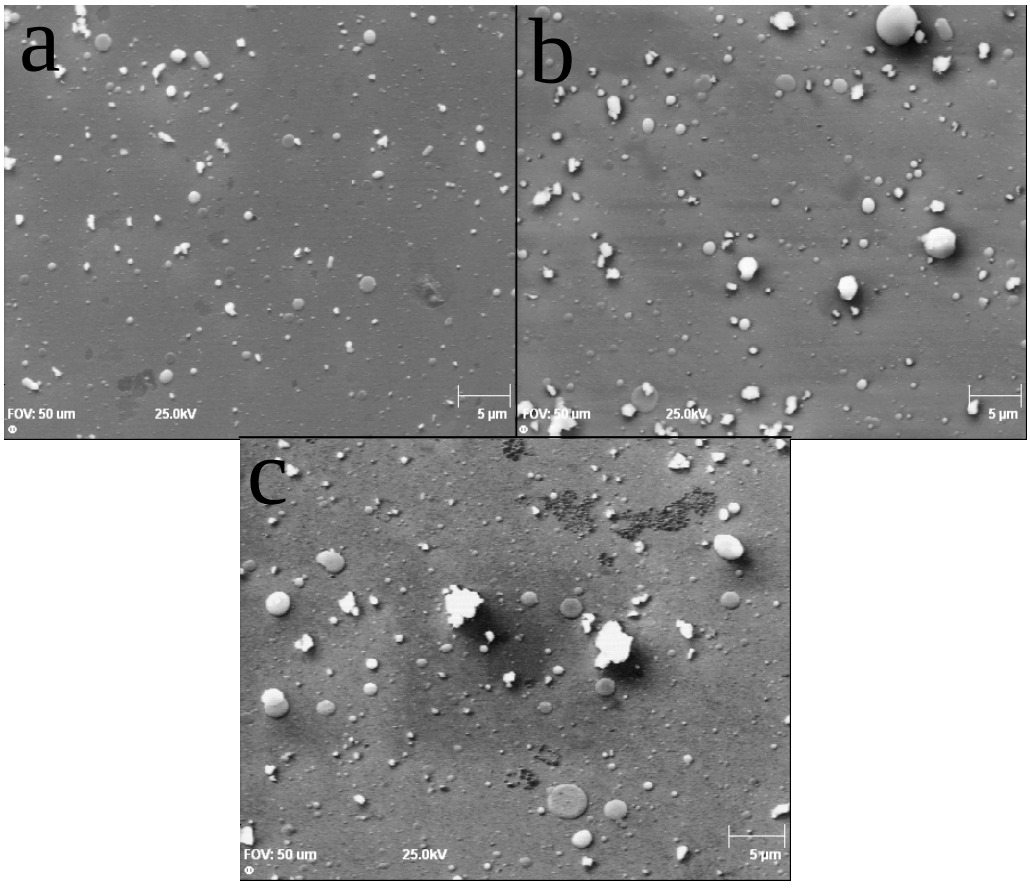

Figure 7.4: SEM micrographs of films ablated in vacuum (a), O2 (b) and Ar (c)

7.4. Conclusion

The pulsed laser deposition (PLD) technique was used to prepare thin films of $Y_3(Al,Ga)_5O_{12}:Ce^{3+}$. Deposition parameters investigated in this chapter includes the substrate temperature, number of pulses and different atmospheres in the chamber. The thickness of the films increased with an increase in the number of pulses from 10 000 pulses to 40 000 pulses, therefore films deposited with 40 000 pulses had the highest PL intensity. Increase in particulate growth was observed with increasing chamber pressure.

7.5. Acknowledgement

This work is based on the research supported by the South African Research Chairs Initiative of the Department of Science and Technology and National Research Foundation of South Africa.

7.6. References

[1] L.C. Chen, “Particulates generated by pulsed laser ablation”. in: D.B. Chrisey, G.K. Hubler Eds.,Pulsed Laser Deposition of Thin Films, Wiley, New York, 1994, p. 167

[2] G. Koren, R.J. Baseman, A. Gupta, M.I. Lutwyche, R.B.Laibowitz, Appl. Phys. Lett. 56 (1990) 2144

[3] K. Murakami, E. Fogarassy, S. Lazare Eds. ,Laser Ablation of Electronic Materials: Basic Mechanisms and Applications, Elsevier, Amsterdam, 1992, p. 125

[4] H. Chiba, K. Murakami, O. Eryu, K. Shihoyama, T. Mochizuki, K. Masuda, Jpn. J. Appl. Phys. 30 (1991) 732

[5] http://www.phosphor-technology.com/products/crt.htm [Accessed 29 May 2012]

[6] S.T.S. Dlamini, H.C. Swart, O.M. Ntwaeaborwa, Sol. State Sci. 23 (2013) 65-71

[7] R. Hansel, S. Allison, G. Walker, J Mater. Sci. 45 (2010) 146-150

[8]P.K. Schenck, M.D. Vaudin, D.W. Bonnell, J.W. Hastie, A.J. Paul, Appl. Surf Sci. 127–129 (1998) 655–661

Chapter 8

Summary and suggestions for future work

8.1. Summary

Ga substitution induced changes in the crystal structure of $Y_3Al_5O_{12}:Ce^{3+}$, these changes are observed in the morphological and luminescence properties. Samples containing Ga have noticeably shorter emission wavelengths (higher energy) and the excitation wavelengths are longer (lower energy). The Ga ion is larger than the Al ion by about 20.5 % in the tetrahedral sites and 17 % in the octahedral sites. The addition of Ga ions into the YAG structure is influential on the environment of the Ce^{3+} ion. Ultimately, the substitution of Ga into the YAG lattice result in a decompression of oxygen atoms directly coordinated to the Ce^{3+} atom and the structure becomes more cubic. This change in structure directly affect the 5d orbitals of the Ce^{3+} and likewise the photoluminescent characteristics. The excitation peaks indicated that Ce^{3+} is excited via the conduction band as well as in the Ce^{3+} ion itself. The two emission peaks confirmed the arrangement of the atom in which the Ce^{3+} can only occupy one lattice side position.

Thin films of the $Y_3Al_5O_{12}:Ce^{3+}$phosphor powder were successfully prepared using the PLD technique. Deposition parameters investigated includes the substrate temperature, number of pulses and different atmospheres in the chamber. Various surface analyzing techniques were used to characterize the morphological and luminescent properties. XRD showed a slight improvement in the crystallization of the films. After the films were annealed, better crystallization of films deposited in an O_2 background was observed. Also the crystallinity of the

films improved with increasing substrate temperature up to 300°C. The crystallinity was affected by interdiffusion at 500°C. The thickness of the films increased with an increase in the number of pulses from 10 000 pulses to 40 000 pulses, therefore films deposited with 40 000 pulses had the highest PL intensity. The films deposited at 300°C also showed the highest PL intensity. High PL intensity was also observed for films deposited in an O_2 background. The results also indicate that deposition conditions of 20 000 pulses, substrate temperature of 300°C in an O_2 atmosphere at 20 mtorr pressure provides good conditions to grow films with high PL intensity and good morphological characteristics. The AES depth profiles indicated the films had different thickness and the distribution of elements on the layer to be homogeneous. AFM images showed nano-meter sized grains and at a 22°C substrate temperature there was a mixture of small grains and large grains. As the substrate temperature was increased to 300°C larger and more uniform grains formed that increased the surface roughness. At 500°C, a decrease in the surface roughness was, however, observed. PL intensity of films with well-defined grains (rougher) surfaces was higher than PL intensity of films characterized by poorly-defined grains (smooth) surfaces. High PL intensity was observed for films deposited in O_2 as compared to those ablated in the Ar atmosphere. PLD proved to be a good technique to grow the films of this phosphor as the RBS data showed that the stoichiometry was maintained from the powder to the film form

8.2. Future work

Future work would include a greater variety of process parameters such as ablation at substrate temperature 200°C, 250°C, 325°, 350°C, 375°C, 400°C and 450°C with the aim of confirming if 300°C is the optimum substrate temperature. Also the ablation can be done in three different gas species (O_2, N_2 and Ar). Ablation in each of the three different gas species at 1 and 3 Torr pressures as well as pressures above 20 mtorr and investigating the effect on the plume. The

effect of the laser energy and target to substrate distance can also be investigated. Annealing of the films after deposition can also be explored more. In this study films were only annealed at 800°C for 2 hours in open air. The PL and morphological properties of the films can be investigated where films are annealed at different temperatures, e.g. 900°C, 1000°C and 1200°C. The duration of the annealing time can be increased as well to 3 and 4 hours. Annealing can also be done in different gas atmospheres such as Ar and N. The use of a different type of the ablation laser can also be of great interest. 266 nm Nd:YAG laser was used in this study. Laser sources of higher energy such as 248 nm KrF and 193 ArF can be used to investigate their influence on the growth of $Y_3(Al,Ga)_5O_{12}:Ce^{3+}$nano thin films. The CL degradation of the films can also be studied: especially the influence of the beam current and beam voltage on the CL degradation. Research following degradation study can be on the coating of the films in order to decrease the degradation rate. One challenge faced when growing thin films is the formation of big unwanted micron particles on the surface. Applying the off axis PLD technique is an option of also trying to minimize the formation of this particles on the surface. This is a technique where the substrate is mounted either upside down in the chamber or at an angle where the plume is not directly focused onto the substrate. Rotating the substrate during the deposition would also aid in uniform thickness growth of the thin films.

9. Publications resulting from this work

- S.T.S. Dlamini, H.C. Swart, J.J. Terblans, O.M. Ntwaeaborwa, The effect of different gas atmospheres on the structure, morphology and photoluminescence properties of pulsed laser deposited $Y_3(Al,Ga)_5O_{12}:Ce^{3+}$nano thin films, Solid State Sciences 23 (2013) 65-71
- S.T.S. Dlamini, H.C. Swart, O.M. Ntwaeaborwa, Photoluminescence properties of Y_3 (Al, Ga)$_5O_{12}:Ce^{3+}$ thin phosphor films grown by pulsed laser deposition, Physica B 439 (2014) 88-92

10. Conference proceedings

- S.T.S. Dlamini, H.C. Swart, O.M. Ntwaeaborwa, Morphological and luminescent properties of $Y_3(Al,Ga)_5O_{12}:Ce^{3+}$ powder phosphor, SAIP'2012 Proceedings, the 57th Annual Conference of the South African Institute of Physics, in press
- S.T.S. Dlamini, H.C. Swart, O.M. Ntwaeaborwa, The effect of substrate temperature on the structure, morphology and photoluminescence properties of pulsed laser deposited $Y_3(Al,Ga)_5O_{12}:Ce^{3+}$ nano thin films, SAIP'2013 Proceedings, the 58th Annual Conference of the South African Institute of Physics, in press

11. Presentations in conferences/workshops

- 57th Conference of South African Institute of Physics - Pretoria (RSA), 9-13 July 2012
  Morphological and luminescent properties of $Y_3(Al,Ga)_5O_{12}:Ce^{3+}$ powder phosphor.
  S.T.S Dlamini, H.C. Swart and O.M. Ntwaeaborwa
- 5^{th} South African Conference on Photonic Materials – Kariega Game Reserve, South Africa 29 April-3 May 2013

Photoluminescence properties of Y_3 $(Al,Ga)_5O_{12}:Ce^{3+}$ thin phosphor films grown by pulsed laser deposition.

S.T.S Dlamini, H.C. Swart and O.M. Ntwaeaborwa

- 58th Conference of South African Institute of Physics – Kwazulu Natal (RSA), 8-12 July 2013

  Morphological and luminescent properties of $Y_3(Al,Ga)_5O_{12}:Ce^{3+}$ powder phosphor.

  S.T.S Dlamini, H.C. Swart, E. Coetsee-Hugo and O.M. Ntwaeaborwa